Assessing the performance of global hydrological models for capturing peak river flows in the Amazon Basin

Jamie Towner[1], Hannah L. Cloke[1,2,4,5], Ervin Zsoter[3,1], Zachary Flamig[6], Jannis M. Hoch[7,8], Juan Bazo[10,11], Erin Coughlan de Perez[9,10], Elisabeth M. Stephens[1]

5 [1]Department of Geography & Environmental Science, University of Reading, Reading, RG6 6AB, UK
[2]Department of Meteorology, University of Reading, Reading, RG6 6BB, UK
[3]European Centre for Medium-Range Weather Forecasts, Shinfield Park, Reading, RG6 9AX, UK
[4]Department of Earth Sciences, Uppsala University, Uppsala, 752 36, Sweden
[5]Centre of Natural Hazards and Disaster Science, CNDS, Uppsala, 752 36, Sweden
10 [6]University of Chicago Center for Data Intensive Science, Chicago, USA
[7]Department of Physical Geography, Utrecht University, P.O. Box 80115, 3508 TC Utrecht, the Netherlands
[8]Deltares, P.O. Box 177, 2600 MH Delft, the Netherlands
[9]International Research Institute for Climate and Society, Columbia University, Palisades, NY 10964, USA
[10]Red Cross Red Crescent Climate Centre, The Hague, 2521 CV, the Netherlands
15 [11] Universidad Tecnológica del Perú (UTP), Lima, Perú

Correspondence to: Jamie Towner (j.towner@pgr.reading.ac.uk)

Abstract. Extreme flooding impacts millions of people that live within the Amazon floodplain. Global Hydrological Models (GHMs) are frequently used to assess and inform the management of flood risk, but knowledge on the skill of available models is required to inform their use and development. This paper presents an intercomparison of eight different GHMs

20 freely available from collaborators of the Global Flood Partnership (GFP) for simulating floods in the Amazon basin. To gain insight into the strengths and shortcomings of each model, we assess their ability to reproduce daily and annual peak river flows against gauged observations at 75 hydrological stations over a 19-year period (1997-2015). As well as highlighting regional variability in the accuracy of simulated streamflow these results indicate that a) the meteorological input is the dominant control on the accuracy of both daily and annual maximum river flows, and b) groundwater and routing

25 calibration of Lisflood based on daily river flows has no impact on the ability to simulate flood peaks for the chosen river basin. These findings have important relevance for applications of large-scale hydrological models, including analysis of the impact of climate variability, assessment of the influence of long-term changes such as land-use and anthropogenic climate change, the assessment of flood likelihood, and for flood forecasting systems.

30 1 Introduction

Flooding is notably the most common and damaging natural hazard affecting millions of people worldwide every year, producing economic losses exceeding billions of dollars (Hirabayashi et al., 2012). Flood risk associated to a particular location can be highly variable depending on levels of exposure, resilience and preparedness (Alfieri et al., 2018) in addition to the increased uncertainty surrounding trends of hydrological extremes in a warming climate (Arnell and Gosling, 2016).

For the Amazon basin, flood risk is considered to have increased, with a greater frequency of extreme flood events (e.g. in 2009, 2012 and 2014; Marengo and Espinoza, 2015) coinciding with a hypothesised intensification of the hydrological cycle since the 1980's (Gloor et al., 2013). Floods in Amazonian communities are known to have large socioeconomic consequences impacting eco-systems, health, transport links and are particularly damaging to agricultural and fishery

5   practices (Schöngart and Junk 2007; Marengo et al., 2012; Marengo et al., 2014; Correa et al., 2017). Single flood events (e.g. 2012 in the Amazonian city of Iquitos, Peru) have impacted the lives of over 73,000 people (IFRC, 2013) with average annual damages estimated at 1.4 billion USD over a four-year period (2008-2011) in the Brazilian Rio Branco river basin alone (Mundial Grupo Banco, 2014).

1.1 Global hydrological models and applications

10   In its simplest form, a hydrological model can be considered a representation of a real-world hydrological system used to better understand various water and environmental processes, predict system behaviour and provide consistent impact assessment (Devia et al., 2015). They work by simulating the hydrological response to meteorological variations incorporating run-off generation and river routing processes (Sutanudjaja et al., 2018). As such, Global Hydrological Models (GHMs) have been used in a wide range of applications including short to extended-range flood forecasting (Alfieri et al.,

15   2013; Emerton et al., 2018), climate assessment (Hattermann et al., 2017), hazard and risk-mapping (Ward et al., 2016), drought prediction (van Huijevoort et al., 2014) and water resource assessment (e.g. water availability models; Meigh et al., 1999; Sood & Smakhtin, 2015).

Depending on the application and the needs of decision makers, different properties of the hydrograph simulated by hydrological models are important. For example, an accurate representation of peak river flows and their likelihood is key

20   for decision-makers who wish to understand the area at risk of flooding. In contrast, estimates of daily streamflow may be more beneficial for the assessment of water resources such as irrigation requirements.

1.2 GHM development

The availability of GHMs has grown in recent years thanks to increased efforts in addressing water related issues in developing countries (De Groeve et al., 2015; Ward et al., 2015; Trigg et al., 2016), the development of flood forecasting

25   systems (Aliferi et al., 2013; Werner et al., 2013; Emerton et al., 2018), improvements within precipitation datasets (Mittermaier et al., 2013; Novak et al., 2014; Forbes et al., 2015), the emergence of new global satellite and remote sensing datasets and advancements in numerical modelling techniques (Yamazaki et al., 2014a; Sampson et al., 2015; Andreadis et al., 2017; Balsamo et al., 2018). For an overview of available GHMs see Bierkens et al. (2015) who have provided the details of 22 large-scale hydrological models with those used for operational flood forecasting being summarised in Emerton

30   et al. (2016).

1.3 Land surface models vs hydrological models

GHMs have differing spatial and temporal resolutions, parameter estimation approaches, number of parameters, calibration methods, input-output variables and overall structure (Sood and Smakhtin, 2015). Their set-ups can generally be divided into two categories: Land Surface Models (LSMs) and hydrological models (Gudmundsson et al., 2012). The majority of LSMs

5   and hydrological models share the same conceptualisation of the water balance (Haddeland et al., 2011) but differ in their objective. LSMs evolve from coupled land/atmosphere models with the purpose of solving the surface energy balance equations to provide the necessary lower boundary conditions to the atmosphere (Wood et al., 2011). In contrast, hydrological models tend to focus less on the partitioning of radiation and more on hydrological resources and understanding the lateral movement and transport of water along the land surface.

10   In terms of differences in model performance, the Gudmundsson et al. (2012) intercomparison study of six LSMs and five GHMs (i.e. hydrological models) concluded that the main differences were due to the snow scheme implemented with snow water equivalent values and mean runoff fractions lower in LSMs. No significant differences between LSMs and hydrological models were found for runoff and evapotranspiration globally but rather the differences between the models themselves created large sources of uncertainty, highlighting the importance of analysing a range of different GHMs rather

15   than a group consisting of a specific model type. For the purposes of this study, we categorise both LSM and hydrological models as GHMs.

1.4 Motivation

For GHMs to be considered effective, end users need to know their accuracy and reliability (Ward et al., 2015). Thus, the evaluation of these models against observed data is an important procedure in efforts to reduce flood risk. Currently, no

20   intercomparison analysis of GHMs has been conducted specifically for the Amazon basin with previous studies focusing solely on the performance of individual models for the Amazon (e.g. Yamazaki et al., 2012; Paiva et al., 2013; Hoch et al., 2017a; Hoch et al., 2017b) or as part of a global study (e.g. Gudmundsson et al., 2012; Alfieri et al., 2013; Hirpa et al., 2018) which lack an in-depth focus on skill within the Amazon basin.

Finally, many of the GHMs (or their components) analysed in this study are used for specific applications. For instance,

25   water resources management (PCRaster Global Water Balance; PCR-GLOBWB), flash flood forecasting (Ensemble Framework for Flash Flood Forecasting; EF5) and extended-range flood forecasting (Global Flood Awareness System; GloFAS). Investigating the performance of hydrological simulations therefore can provide valuable information to researchers and model developers with which to better understand some of the strengths and weaknesses which exists within the model set-ups and help to distinguish how different parts of the hydrological chain can cause particular 'good' or 'bad'

30   model performance; thus, having implications for their different applications.

1.5 Objectives

In this study, the main objective is to assess the ability of different GHMs freely available from collaborators within the Global Flood Partnership, (GFP) identifying which approaches are most suitable in different areas of the Amazon basin for simulating flood peaks. To pursue this objective, the analysis is designed to answer the following research questions:

5 1. How well do GHMs represent the annual hydrological regime in terms of the Kling-Gupta-Efficiency (KGE) and its individual components?
2. Which model set-up best represents annual maximum river flows?
3. Which hydrological routing model allows the best representation of daily and peak river flows?
4. Which precipitation dataset allows the best representation of daily and peak river flows?
10 5. How do results differ when using a LSM as opposed to a hydrological model?
6. By how much does calibration of groundwater and routing model parameters improve performance?

2 Data and methodology

The experimental design involves comparing the output of daily and annual maximum discharge estimates produced by different GHMs forced using atmospheric reanalysis or satellite precipitation datasets against observations of streamflow.

15 The common validation period is 1997-2015 with results also analysed for the shorter period of 2004-2015 to account for the shorter record length of one simulation.

2.1 Observations

Observed daily discharge data is used to evaluate each of the model runs. The network of hydrometric gauges is controlled and maintained by the national institutions responsible for hydrological monitoring in countries situated within the Amazon

20 basin. These include: Agência Nacional de Águas (Water National Office – ANA, Brazil), Servicio Nacional de Meteorología e Hidrología (National Meteorology and Hydrology Service – SENAMHI, Peru and Bolivia), Instituto Nacional Meteorologia e Hidrologia (Institute to Meteorology and Hydrology, INAMHI, Ecuador) and the Instituto de Hidrología, Meteorología y Estudios Ambientales (Institute of Hydrology, Meteorology and Environmental Studies - IDEAM, Colombia).

25 Daily water level values are collected by the respective institution and are sourced through the ORE-HYBAM observational service (see http://www.ore-hybam.org/) or directly from the national services. A time series of daily river flow for each station is obtained using stage and rating curve measurements which were determined using an acoustic Doppler current profiler (ADCP) conducted by the ORE-HYBAM observatory and SENAMHI (Espinoza et al., 2014). In total 75 hydrological stations throughout the Amazon basin are selected with an average record length of 17 years within the main

30 validation period (1997-2015). The locations of stations and their characteristics are displayed in Fig. 1a and Table S1

respectively. Stations selected have a minimum of five consecutive years' worth of data during the main validation period. The threshold was set to five to prevent the elimination of stations in data scarce areas such as Peru, Bolivia and Colombia.

2.2 Routing models and meteorological datasets

Eight GHMs composed of different meteorological datasets, hydrological/LSMs and river routing models, are used to each

5 simulate river discharge across the Amazon basin. Four meteorological products (ERA-Interim Land re-analysis, ERA-5 re-analysis, ECMWF 20-year control reforecasts (hereafter used as reforecasts) and the real-time TRMM TMPA 3B42 v.7), three hydrological/LSM (PCR-GLOBWB, the Hydrology-Tiled ECMWF Scheme for Surface Exchanges over Land; H-TESSEL, EF5) and three river routing models (Catchment-based Macro-scale Floodplain model; CaMa-Flood, Lisflood and the Coupled Routing and Excess Storage; CREST) are employed. While the focus of this study is on GHMs made available

10 by the GFP community, other models are available within the Amazon basin. Some examples include: MGB-IPH (Paiva et al., 2013), LPJmL (Lund–Potsdam–Jena managed Land; Bondeau et al., 2007), WaterGAP (water - global analysis and prognosis; Döll et al., 2003) and MAC-PDM.09 (the Macro-scale-Probability-Distributed Moisture model.09; Gosling & Arnell, 2011).

As a result of using freely available datasets from collaborators within the GFP, simulations are composed of a combination

15 of routing models and meteorological datasets and do not all use the same precipitation input or hydrological set-up. However, the available combinations allow enough insight into the model components to draw conclusions for the objectives stated. For example, to analyse the performance of precipitation inputs, ERA-Interim Land, ERA-5 and the reforecasts are forced through the calibrated version of Lisflood whereby the routing and LSM remain consistent. To evaluate the differences between using the Lisflood and CaMa-Flood routing models two simulations which use ERA-Interim Land

20 precipitation and the LSM H-TESSEL are compared. To identify the differences between employing a hydrological (PCR-GLOBWB) or LSM (H-TESSEL), two set-ups which use the ERA-Interim Land precipitation reanalysis and the CaMa-Flood river routing model are directly compared. Finally, to see how much benefit model calibration within Lisflood provides, ERA-Interim Land and ERA-5 are forced through the calibrated and un-calibrated Lisflood model versions. The CREST EF5 run is the sole simulation to have a unique hydrological model and meteorological input and although it is more

25 challenging to analyse the performance of specific components of the model set-up against other simulations, it was included in the analysis for completeness.

An alternative approach would be to implement a full intercomparison experiment and run a new set of simulations which included all combinations of precipitation input, GHM and routing scheme. However, this is a very large undertaking and the time and computational expense to achieve this is prohibitive. Instead, by using freely available datasets with different

30 hydrological set-ups, our method allows a first analysis providing enough evidence of dataset reliability and accuracy in order to determine the utility of the differing approaches for climate studies and to forecast applications. Moreover, by using iterative runs of similar model set-ups (i.e. changing a specific part of the hydrological model chain) it allows us to make

conclusive statements regarding the differences in skill. Finally, a short description of each model and atmospheric product is outlined below with a summary of each simulation provided in Table 1.

2.2.1 Precipitation datasets

ERA-Interim Land is a global reanalysis of land surface parameters produced by the European Centre for Medium-range
5   Weather Forecasts (ECMWF) with a T255 spectral resolution (~80 km or ~0.75^0) (Balsamo et al., 2015). ERA-Interim Land was produced using the latest version of the land surface H-TESSEL model using atmospheric forcing from ERA-Interim (Dee et al., 2011), with precipitation adjustments based on the Global Precipitation Climate Project (GPCP) v2.1. Precipitation improvements were achieved by Balsamo et al. (2010) using a scale-selective rescaling procedure in which ERA-Interim 3-hourly precipitation were corrected to match the monthly accumulation provided by the GPCP at grid point
10   scale (Huffman et al., 2009). All simulations which use ERA-Interim Land are run offline to force the associated rainfall-runoff models (see Table 1). For a detailed description of the ERA-Interim Land and ERA-Interim datasets see Balsamo et al. (2015) and Dee et al. (2011) respectively. Dataset available at: <http://apps.ecmwf.int/datasets/data/interim-full-daily/levtype=sfc/>.

ERA-5 is the latest reanalysis product of the ECMWF producing consistent estimates of atmospheric, land and ocean
15   variables at a horizontal resolution of ~31 km while the vertical atmosphere is discretised into 137 levels to 0.01 hPa (ECMWF, 2018). ERA-5 is based on the Integrated Forecasting System (IFS) Cycle 41r2 which was used operationally at the ECMWF in 2016. Early analysis has shown that ERA-5 has an improved representation of precipitation (particularly over land in the deep tropics), evaporation and soil moisture compared to its predecessor ERA-Interim Land (ECMWF, 2017). ERA-5 is currently being produced in three "streams" and will eventually cover the period 1950 to near real-time (~3
20   days) with completion due in 2019 (Emerton et al., 2018). Dataset available at: <https://software.ecmwf.int/wiki/display/CKB/How+to+download+ERA5+data+via+the+ECMWF+Web+API>

ECMWF reforecasts are a collection of historical forecasts from start dates at the same day of the year going back for a specific number of years to provide a consistent model climatology from which to compare forecasts (ECMWF, 2016). In this study we use the control member of the reforecasts which are created based on a retrospective run of the most recent
25   version of the ECMWF's IFS to provide surface and subsurface runoff as input to the Lisflood routing model at a resolution of 0.1^0. The reforecast run is computed using a lighter configuration (11 ensemble members, run twice a week on Mondays and Thursdays) to reduce computational time. The purpose of running the ECMWF forecasts through the Lisflood routing model is to generate a long term (20-year) dataset which is consistent with operational GloFAS forecasts enabling the suitability of the dataset for use in the calibration of the Lisflood model parameters (Hirpa et al., 2018). This data covers the
30   period June 1995 to June 2015 and due to frequent model updates of the IFS is based on multiple model cycles: Cycle 41r1 (July through March) and Cycle 41r2 (March through June). The control reforecasts from Mondays and Thursdays are used subsequently to fill the whole weeks by taking the first 3 and 4-day forecast periods respectively throughout the 20 years.

TRMM TMPA 3B42 RT v7 is a global merged multi-satellite precipitation product generated at the National Aeronautics and Space Administration (NASA). TMPA is computed for two products: a near real-time version (TMPA 3B42RT v7) and a post real-time gauged adjusted research version (TMPA 3B42 v7), both of which run at resolution of 3 hourly x 0.25^0 x 0.25^0 (Huffman et al., 2007). The TMPA 3B42 RT gridded dataset used in this study covers the global latitude belt from 60^0

5 N to 60^0 S. For further information see Huffman et al. (2007). Dataset available at: < https://pmm.nasa.gov/data-access/downloads/trmm>.

2.2.2 Hydrological and land surface models

H-TESSEL provides the land surface component of the ECMWF IFS (van den Hurk et al. 2000; van den Hurk and Viterbo 2003; Balsamo et al. 2009). H-TESSEL simulates the land surface response to atmospheric conditions estimating water and

10 energy fluxes (heat, moisture and momentum) on the land surface (Zsoter et al., in review). H-TESSEL is predominately used within the operational set-up of short to seasonal-range weather forecasts coupled with the atmosphere, but it can also be used in an "offline mode" to calculate the land surface response to atmospheric forcing, whereby input data (e.g. near surface meteorological conditions) is provided on a 3 hourly timestep (Pappenberger et al., 2012). In this study, H-TESSEL receives boundary conditions from the atmospheric input provided by either the ERA-5 reanalysis, ERA-Interim Land

15 reanalysis or the reforecasts providing total runoff for the CaMa-Flood routing model, and the surface and sub-surface water fluxes for Lisflood. Runs forced using the ERA-Interim Land reanalysis are run in the offline mode. For a detailed description of H-TESSEL see Balsamo et al. (2009).

PCR-GLOBWB is a global hydrological and water resource model developed at the Department of Physical Geography, Utrecht University, Netherlands (Sutanudjaja et al., 2018). For each grid cell and time step, PCR-GLOBWB simulates

20 moisture storage in two vertically stacked upper soil layers, as well as the water exchange among the soil, the atmosphere, and the underlying groundwater reservoir. Besides, water demands for irrigation, livestock, industry, and households can be integrated within the model. Run-off is routed along a Local Drainage Direction (LDD) network using the kinematic routing wave equation. PCR-GLOBWB was applied at a resolution of 30 arcmin (~ 55km x 55km at the Equator) with meteorological forcing provided from the ERA-Interim Land reanalysis dataset between 1997 and 2015. For further

25 information on PCR-GLOBWB, see van Beek and Bierkens (2008), van Beek et al. (2011) and Sutanudjaja et al. (2018).

EF5 is an open source software package developed at the University of Oklahoma (OU) that consists of multiple hydrological model cores producing outputs of streamflow, water depth and soil moisture (Clark et al., 2016). Since 2016, EF5 has been used operationally for local forecasts across the U.S. National Weather Service (NWS) for flash flooding purposes (Gourely et al., 2017). EF5 incorporates CREST which is a distributed hydrological model created by OU and

30 NASA (Wang et al., 2011). Within CREST, runoff generation, evapotranspiration, infiltration and surface and subsurface routing are computed at each grid cell within the model domain with surface and subsurface water routed using a kinematic wave assumption. Four excess storage reservoirs characterise the vertical profile within a cell representing interception by

the vegetation canopy and subsurface water storage in the three soil layers (Meng et al., 2013). In addition, the representation of sub-grid cell routing and soil moisture variability is made through the use of two linear reservoirs for overland and subsurface runoff individually (Wang et al., 2011). Locations of major streams, flow direction maps and flow accumulation are all derived from the HydroSHEDS dataset (Lenhnar et al., 2008).

5   In this study, an un-calibrated version of EF5 was run using CREST version 2.0 (Xue et al., 2013; Zhang et al., 2015) for 13 years (2003-2015) with a one-year spin-up at a spatial resolution of 0.05^0 x 0.05^0. Parameters are estimated a priori from soil and geomorphological variables with meteorological forcing provided by the TMPA 3B42 RT product for precipitation and monthly averaged potential evapotranspiration (PET) from the Food and Agriculture Organisation (FAO). For full details on the system set-up see Clark et al. (2016).

10   ### 2.2.3 Routing models

Lisflood is a global spatially distributed, grid based hydrological and channel routing model commonly used for the simulation of large-scale river basins (van Der Knijff et al., 2010). It is currently used as an operational rainfall-runoff model within the European Flood Awareness System (EFAS) for streamflow forecasts over Europe (Smith et al., 2016). Unlike EFAS, which uses the full Lisflood set-up, GloFAS and the simulations included in this study use only the routing

15   component of the Lisflood set-up with surface and sub-surface input fluxes (e.g. vertical water, water/snow storage) provided by the H-TESSEL module of the IFS at a resolution of 0.1^0. Surface runoff is routed through Lisflood using a four-point implicit finite-difference solution of the kinematic equations. Sub-surface storage and transport is routed to the nearest downstream channel pixel within one-time step through two linear reservoirs (Alfieri et al., 2013). The water in each channel pixel is finally routed through the river network taken from the HydroSHEDS project (Lenhnar et al., 2008) using the same

20   kinematic wave equations as for the overland flow. Subsurface flow from the upper and lower groundwater zones is routed into the nearest downstream channel as a scaled sum of the total outflow from both the upper and lower groundwater zones. Further details of the Lisflood model is described in van der Knijff et al. (2010).

In this study, two set-ups of Lisflood are used (Lisflood_uc and Lisflood_c). Lisflood_c represents the calibrated set-up of the Lisflood routing and groundwater parameters (see Hirpa et al., 2018). Parameters were calibrated with the reforecasts

25   initialised with the ERA-Interim land reanalysis from 1995-2015 as forcing, against observed discharge data at 1278 gauging stations worldwide. All but one station (*40*, see Fig. 1a & Table S1) used in this study were included within the calibration. An evolutionary optimization algorithm was used to perform the calibration with the Kling-Gupta Efficiency (KGE) as the objective function. The calibration was carried out for parameters controlling the time constants in the upper and lower zones, percolation rate, groundwater loss, channel Manning's coefficient, the lake outflow width, the balance between

30   normal and flood storage of a reservoir and the multiplier used to adjust the magnitude of the normal outflow from a reservoir. The results were validated by Hirpa et al. (2018) using the Kling Gupta Efficiency (KGE; Gupta et al., 2009) over the period 1995-2015. In calibration (validation) KGE skill scores were greater than 0.08 compared to the default Lisflood

simulation for 67% (60%) of stations globally. For a detailed description of the calibration of the Lisflood parameters and the range of values used for each parameter see Hirpa et al. (2018).

CaMa-Flood is a global distributed river routing model which is forced by runoff input from a LSM or hydrological model to simulate water storage where further hydrological variables (i.e. river flow, water level and inundated area) can be derived along a prescribed river network. Horizontal water transport along the river network is calculated using the local inertia equations (Yamazaki et al., 2011). The backwater effect (i.e. upstream water levels which affect flow velocity downstream, see Meade et al., 1991) is represented by estimating flow velocity based on water slope. (Yamazaki et al., 2011). Moreover, floodplain inundation is represented within CaMa-Flood as a subgrid scale process by discretising the river basin into unit catchments which consist of subgrid river and floodplain topography parameters (Yamazaki et al., 2014b). These parameters describe the relationship between the total water storage in each grid point and water stage and are automatically generated using the Flexible Location of Waterways (FLOW) method with the generation of the river map created by upscaling the HydroSHEDS flow direction map (Lehner et al., 2008). For further information about the CaMa-Flood model see aforementioned references. In this study, daily river discharge was obtained using CaMa-Flood version 3.6.1 at a spatial resolution of 0.25^0 (~25km grid size) for both runs. The Manning's river and floodplain roughness coefficients were set at $0.03 \text{ s m}^{-1/3}$ and $0.10 \text{ s m}^{-1/3}$ uniformly for both CaMa-Flood simulations.

2.3 Verification metrics

2.3.1 Spearman's ranked correlation

The non-parametric Spearman's rho is used to measure the strength and direction of the monotonic relationship between the ranks of the observed and simulated annual maximum values. The non-parametric Spearman's rho was preferred to the Pearson's statistic as non-parametric measures are less sensitive to outliers in the data and are widely considered a more robust measure of the correlation between observed and predicted values (Legates & McCabe, 1999). Correlation scores for rho range from -1 to 1 with 1 being a perfect correlation. We consider scores which have a value of 0.6 or more to be considered skilful. Similar scores (between 0.5-0.7) are considered to represent a good level of agreement between observed and simulated values in similar studies (see Yamazaki et al., 2012; Alfieri et al., 2013).

2.3.2 KGE

The KGE (Gupta et al., 2009) measures the goodness-of-fit between estimates of simulated discharge and gauged observations and is a modified version of the dimensionless Nash Sutcliffe Efficiency (NSE; Nash and Sutcliffe, 1970). The metric decomposes the NSE into three independent hydrograph components (linear correlation (r), bias ratio (β) and relative variability between the observed and simulated streamflow (α)) by re-weighting the relative importance of each (Revilla-Romero et al., 2015). KGE values range from - ∞ to one with values closer to one indicating better model performance.

When analysing the results, each component of the KGE is also considered independently enabling model errors to be directly related to either the variability (KGE_ α), bias ratio (KGE_ β) or correlation (KGE_r) (Guse et al., 2017). KGE_α values greater than 1 indicates that variability in the simulated time series is higher than that of the observed. Values less than 1 show the opposite effect. KGE_ β values greater than 1 indicate a positive bias whereby predictions overestimate

5 flows relative to the observed data while values less than 1 represent an underestimation.

To evaluate the relative improvement of using one model set-up relative to another (e.g. using the calibrated Lisflood routing model as opposed to the uncalibrated model version) metrics are calculated as skill scores:

$$KGE_{SS} = \frac{KGE_a - KGE_{def}}{1 - KGE_{def}}$$ (1)

Where: KGE_{SS} signifies the KGE skill score, KGE_a is the KGE score for the improved run or simulation of interest (e.g.

10 Lisflood_c) and KGE_{def} is the KGE score for the 'default' or comparative run (e.g. Lisflood_uc). Positive KGE_{ss} indicates improved skill whilst a negative score represents a decrease in skill. For each case, KGE scores are calculated against observed river flow data. The correlation skill score is calculated similarly. All metrics are computed in the R environment using the 'verification' (Gilleland, 2015) and 'hydroGOF' (Zambrano-Bigiarini, 2017) R-packages.

3 Results and discussion

15 To allow for easier interpretation, the results and discussion are separated into six sections which match the research questions presented in Sect. 1.5 in addition to an outline of potential future work. Due to similar results between the two validation periods (1997-2015 and 2004-2015), only results for 1997-2015 are shown. For 2004-2015 results see Figs. S1 & S2. Results and discussions for individual stations are commonly referred to by the station numbers in italics and are presented in Fig. 1a and Table S1.

20 **3.1 How well is the annual hydrological regime represented?**

The annual hydrological regime on average is well represented by all models (Fig. 2) with the rationale for poorer performance at specific gauges dependent on each model based on either the temporal correction, bias ratio or variability ratio components of the KGE (Figs. 3-5). An average of 81% of stations are considered skillful (i.e. > 0) for the KGE metric across all eight simulated runs with a maximum value of 0.92 observed at the Santa Rosa gauging site (*48*, Fig. 1a) for the

25 ERA-5 Lisflood_c simulation (Fig. 2f). The two CaMa-Flood set-ups using the hydrological model PCR-GLOBWB and the LSM H-TESSEL show the lowest skill with 48 and 52 stations noting positive scores respectively. On the contrary, best performance is from the calibrated Lisflood set-ups with average station scores of 0.37, 0.41 and 0.53 for runs forced with ERA-Interim Land, ERA-5 and the reforecasts respectively. Such results are unsurprising given that the KGE was used as the objective function in the calibration algorithm of the Lisflood routing model.

In terms of spatial distribution, poorest performance is consistent for the majority of simulations at the Arapari (*55*), Boca Do Inferno (*56*) and Base Alalau (*61*) gauging stations located north of Manaus, at the Fazenda Cajupiranga gauge (*64*) in the northernmost Branco catchment and at the Fontanilhas (*35*) and Indeco (*49*) stations in the south-eastern Brazilian Amazon (Fig. 2).

5   In the south-eastern Amazon, particularly in the Madeira and Tapajos sub-basins, the quantity of existing or under construction dams is at its highest (Fig. 1b). Damming of rivers is known to have impacts on different aspects of the flow regime with possible alterations in the timing, magnitude and frequency of low and high flows (Magilligan & Nislow, 2005). Indeed, the frequency and duration of low and high flow pulses at stations downstream of dams has been shown to be particularly affected by the construction of cumulative dams (Timpe & Kaplan, 2017). Thus, discrepancies between observed

10 modelled and observed data shown in Fig. 2 could be due to alterations to key features of the flow regime.

Highest scoring stations (KGE score > 0.7) are predominately in the south-western Brazilian Amazon where the network of tributaries remain unaffected by damming. However, high skill at stations (*32*, *33* & *43*) along the Madeira river for most simulations (Fig. 2) highlight that the impacts of hydroelectric dams needs to be considered on an individual basis with two of the largest dams (> 3000 MW) situated along the river (see Fig. 1b).

15 Figures 3, 4 and 5 show the breakdown of the KGE scores for each hydrological component to evaluate differences in performance with respect to the correlation (i.e. timing), flow variability (α) and bias ratio (β). An average of 79% of stations note correlation coefficients exceeding 0.6 across all runs with those using the Lisflood routing model performing similarly in both spatial distribution and magnitude (Fig. 3). In contrast, 51% and 47% of stations achieve values exceeding 0.6 for CaMa-Flood H-TESSEL and CaMa-Flood PCR-GLOBWB respectively with the hydrological model, PCR-GLOBWB

20 noting better performance at stations along the main-stem. The increased performance of Lisflood relative to simulations incorporating CaMa-Flood are likely due to the increased spatial resolution (see Table 1). This is supported by results for CREST EF5 with 76% of stations noting values above 0.6 with the resolution again much higher than that of the CaMa-Flood routing scheme (Fig. 3g).

The variance of modelled river flow is on average higher than the observed time series in all of the simulations with the

25 exception of ERA-Interim Land PCR-GLOBWB CaMa-Flood. For this run, 85% of stations observe values less than one with stations situated in the Peruvian Amazon (*2*, *3*, *4* and *5*) the notable exception (Fig. 4b). In contrast, 79% of stations for CaMa-Flood set-up using the LSM H-TESSEL note values greater than one (Fig. 4a).

All runs tend to underestimate river flows relative to the observed time series with the majority of stations observing a beta value below one (Fig. 5). Almost half of all stations using the calibrated Lisflood routing model forced with the reforecasts

30 achieve scores between 0.9 and 1.1 (i.e. grey circles) with the average between stations being exactly one (Table 2). These results are not replicated in the other two calibrated simulations when using either ERA-Interim Land or ERA-5 (Figs. 5d &

5f) with a decrease found in the number of stations observing scores between 0.9 and 1.1 relative to the associated uncalibrated Lisflood set-ups (Figs. 5c & 5e).

Stations in the south-eastern Amazon, particularly in the upper reaches of the Teles Pires river (*37, 38 & 49*), tend to underestimate river flow for most simulations (Fig. 5). In this region of the basin precipitation is controlled by frontal
5   systems in the South Atlantic Convergence Zone (SACZ) which is prevalent during austral summer (Ronchail et al., 2002; Espinoza et al., 2009). Further analysis could be useful in evaluating seasonal patterns of model performance to establish whether climatological features such as the SACZ are accurately represented within the precipitation datasets.

The KGE allows us to make explicit interpretations into the hydrological performance of each model owing to decomposition into correlation, bias and variability terms (Kling et al., 2012). The results indicate that the required
10   developments to improve the representation of daily river flows is specific to each individual model and to the area of interest. For instance, for the ERA-Interim Land PCR-GLOBWB run, daily correlation scores (Fig. 3b) showed the model suffers at reproducing the temporal dynamics of flow (as measured by r) in northern catchments. Calibration of parameters which control the timing of the flood wave (e.g. river flow velocity) may improve performance. Whereas, model set-ups incorporating the uncalibrated Lisflood routing model generally had lower KGE values in the east of the basin corresponding
15   to an overestimation of river flow variability (Figs. 2c & 4c). For these runs, performance slightly improved upon the calibration of the groundwater and routing parameters relating to timing, flow variability and groundwater loss (Figs. 2d & 4d).

3.2 Which model set-up best represents annual maximum river flows?

Both the calibrated and uncalibrated versions of Lisflood simulations forced with the ERA-5 dataset are the best performing
20   runs with average correlation coefficients of 0.48 for both (Fig. 7 & Table 2). However, a large deterioration in skill is evident for all simulations for Spearman's ranked coefficients between observed and predicted annual maximum river flows (Fig. 6) with only 21% of stations on average observing scores exceeding 0.6 across all simulations. Here, it is important to note that due to the length of some station time series the number of overlapping data points can be small and therefore the spatial distribution of model performance should be interpreted with caution. To provide a certain level of confidence
25   between results, stations whose time series equals or exceeds 15 years are denoted using a circle whereas those between 10-14 and 5-9 are represented using a square and triangle respectively.

Highest scores are generally located towards the eastern side of the basin around the mouth of the Amazon River, though these are constrained to runs using the Lisflood routing model with either ERA-Interim Land or ERA-5 as forcing (Fig. 6c-f). Interestingly, the Lisflood set-up forced using the reforecasts does not replicate scores in this region (Fig. 6h) indicating
30   that the error between simulated and observed peak river flows could be associated with the precipitation. However, when comparing results of ERA-Interim H-TESSEL CaMa-Flood and the ERA-Interim Land H-TESSEL Lisflood_uc set-ups,

correlations are much lower in the CaMa-Flood simulation suggesting that both precipitation and routing processes are equally important (Figs. 6a & 6c).

Low agreement between peaks is consistent in the south-east and north-west of the basin across all simulations (Fig. 6). In the south-east, a lack of skill could again be associated with the abundance of hydroelectric dams in the region or through the

5   poor representation of the SACZ rainfall regime. Evaluating the ability to represent the timing and magnitude of the annual flood wave has important implications for models predicting flood hazard and for practices providing early warning information. These results identify that while the representation of daily river flows improves upon model calibration of the Lisflood routing model (Sect. 3.1), the influence of routing calibration for simulating flood peaks has no impact.

3.3 What is the best performing hydrological routing model?

10   We assessed the performance of the CaMa-Flood and Lisflood_uc routing models by comparing the two runs which are forced using the ERA-Interim Land reanalysis dataset. On average the uncalibrated Lisflood run outperforms CaMa-Flood for all metrics analysed with the exception of the bias ratio component of the KGE (Table 2). Results from the EF5 CREST model are also discussed but are not directly comparable due to differing meteorological inputs.

Scores from the correlation component of the KGE are found to increase on average by 0.18 when using the un-calibrated

15   Lisflood model relative to CaMa-Flood with 28 more stations achieving a correlation score of 0.6 or higher (Figs. 3a & c). This number increases when considering correlation scores greater than 0.8 with 38 and seven stations reaching this value for Lisflood and CaMa-Flood respectively. The most notable increase in skill is found in Peru along the Marañón and Napo rivers (*2 & 5*) which note an increase of 0.85 and 0.71 respectively when using the Lisflood model. In comparison the EF5 CREST simulation fits between the CaMa-Flood and Lisflood runs with an average daily correlation score of 0.65 while 12

20   stations achieve scores greater than 0.8 (Fig. 3g).

For the overall KGE metric, 69% of stations have positive values for CaMa-Flood and 24% are found to exceed 0.5. These figures rise to 83% and 52% respectively in the Lisflood run. Large differences are particularly notable at stations situated in the upper reaches of the Solimões River (*2-6*) and within a cluster of stations situated towards the Colombian Amazon in the north-west (Fig. 2c). Results from the EF5 CREST model again fit between CaMa-Flood and Lisflood with 77% and 40% of

25   stations exceeding zero and 0.5 respectively and a median score close to that of Lisflood (Fig. 7c). Larger differences are identified for peak flow correlations with only three stations (*27*, *17* and *22*) achieving scores exceeding 0.6 for the CaMa-Flood simulation compared to 22 using the uncalibrated Lisflood routing scheme (Figs. 6a & 6c). In comparison, the CREST EF5 simulation has 11 stations exceeding this threshold with no distinguishable pattern (Fig. 6g). For this run, the time series of modelled data is shorter (2004-2015) and so peak flow correlations should be interpreted with caution.

30   Zhao et al. (2017) concluded the importance in the choice of river routing scheme for simulating peak discharge across the globe while Hoch et al. (2017b) comparison of two routing models found results to differ despite having identical boundary

conditions. It is therefore of interest to evaluate not only the entire GHM set-up but also the suitability of each model component of the hydrological chain to determine which routing model is most suitable for certain applications within the Amazon basin. Differences in skill for the KGE results is likely associated to the correlation (i.e. timing) with a similar mean and median for the variability and bias ratio (Table 2 and Fig. 7). This suggests that adjustments of parameters such as the

5 Manning's channel coefficient could potentially improve the performance of the CaMa-Flood model with the default coefficient higher in the uncalibrated Lisflood set-up (0.10 as opposed to 0.03; see Hirpa et al., 2018 for all default parameter values).

3.4 What is the best performing precipitation dataset?

Three precipitation products (ERA-Interim Land, ERA-5 and the reforecasts) are used to force the calibrated Lisflood

10 routing model with the most recent ERA-5 reanalysis product the best performing dataset. When comparing observed and simulated annual peak flows, correlation scores improve by an average of 0.11 and 0.15 when using ERA-5 compared to using ERA-Interim Land and the reforecasts respectively (Table 2). 28 stations reach the 0.6 threshold compared 22 and nine stations for ERA-Interim Land and the reforecasts respectively with the range of coefficients smaller for ERA-5 (Fig. 7a).

Figures 8e and 8f highlight the relative gain or loss in skill when using ERA-5 compared to ERA-Interim Land. Greatest

15 improvements for each metric are observed within the upstream reaches of the Solimões River, particularly for stations located within the Peruvian Amazon (*2*, *4* & *5*). In the main western headwater to the Solimões River (the Marañón river) at the San Regis gauging site (*2*) and at Tamshiyacu (*4*) near to the city of Iquitos the annual maximum correlation skill scores are 0.51 and 0.59 respectively. These results highlight that poor performance found in upstream reaches of the Solimões River (Fig. 6c & 6d) is likely due to the representation of rainfall rather than routing performance.

20 In the other main tributary to the Solimões River, the Ucayali river, simulated annual peak flows show little agreement with observed data with a decrease in skill identified when using ERA-5 as opposed to ERA-Interim Land (Fig. 8e). Despite the lack of agreement between observed and modelled data in the Ucayali river the higher correlation scores identified downstream at Tamshiyacu suggests that better representation of high-water periods at the start of the Solimões River is likely modulated by the larger Marañón river. Therefore, our ability to represent flood hazard in communities near to the city

25 of Iquitos is more dependent on how well we can predict river flow in the Marañón river.

All three runs perform well for the KGE metric with little difference in results spatially. The reforecast run used within the Lisflood calibration is found to be slightly superior with 91% of stations achieving scores above zero relative to 88% with ERA-Interim Land and ERA-5. Differences between ERA-Interim Land and ERA-5 become more evident when observing scores exceeding higher thresholds with nine more stations scoring above 0.5 for ERA-5. Increased skill in the Peruvian

30 Amazon is again the most noteworthy (Fig. 8f) with KGE skill scores of 0.67 for the Requena (*3*) (Ucayali river) and San Regis (*2*) (Marañón river) stations and 0.71 for Tamshiyacu (*4*) (Solimões River) when using ERA-5 relative to ERA-Interim

Land. This increase in KGE skill can be attributed to an improvement in the variability and bias ratios found between the simulated and observed time series. Daily correlation scores for the three stations (*2, 3 & 4*) are near identical with the variance and bias underestimated for ERA-Interim Land while being much closer to the observed data for ERA-5 (Figs. 4d,f & 5d,f).

5   The Tamshiyacu gauging station (*4*) is used to measure flood hazard in the city of Iquitos at the start of the Solimões River (Espinoza et al., 2013) and is therefore of particular interest. At this important location, scatterplots of observed against simulated river discharge (Fig. 9) show that the negative bias observed when using ERA-Interim Land reanalysis is corrected when using ERA-5 with the magnitude of 90th percentile river flows almost identical to that of the observed dataset. Improvement is likely associated with the increased resolution of the ERA-5 reanalysis. Waters found at Tamshiyacu are of

10   Andean origin meaning that the representation of rainfall in the Andes Mountains is fundamental to accurately predicting streamflow. ERA-5 runs at a horizontal resolution of ~32 km and includes an additional 73 vertical levels to 0.01 hPa compared to ERA-Interim Land, meaning the representation of the troposphere is enhanced.

The success of GHMs in producing adequate estimates of river flow is underpinned by uncertainties within the meteorological input (Butts et al., 2004; Beven, 2012; Sood & Smakhtin, 2015). These results have particular importance for

15   flood forecasting applications and research concerning extreme floods with the higher resolution ERA-5 dataset providing closer agreement between observed and simulated annual maximum river flows, particularly for the Peruvian Amazon. With the time series of observed data often beginning in the 1980's in the Amazon, ERA-5 could provide a useful tool for analysing historical flows and establishing links to climate variability. Upon completion, ERA-5 will date back to 1950 (Zsoter et al., in review) meaning locations in which model skill is considered high could benefit from up to 30 years' worth

20   of additional data for use in climate studies allowing for more robust analysis.

3.5 How do results differ between using a LSM and a hydrological model?

The LSM, H-TESSEL and the hydrological model, PCR-GLOBWB were directly compared whereby the precipitation forcing (ERA-Interim Land) and river routing scheme (CaMa-Flood) were consistent. Overall, it appears that the choice between using a LSM or a hydrological model in the Amazon basin is dependent not only on the specific region of interest

25   but also on the application and needs of the user. Previous studies (Zhang et al., 2016; Beck et al., 2017) have found that LSM models, on average, perform better in rainfall dominant regions, whereas hydrological models tend to achieve better results in snow dominated regions owing to the use of complex energy balance equations introducing additional uncertainties. For the Amazon basin, the average Spearman's rank correlation coefficients between simulated and observed peak river flow is slightly higher for the LSM with scores of 0.25 and 0.19 respectively (Table 2). However, the number of

30   stations with Spearman's maximum correlation scores exceeding 0.6 is higher in PCR-GLOBWB at nine compared to just three with H-TESSEL (Figs 6a & 6b).

To illustrate the gain or loss in skill when using the LSM relative to PCR-GLOBWB the Spearman's annual maximum correlation and KGE skill scores were calculated for each station (Figs. 8g & 8h). Overall, 68% of stations show improved skill for peak river flow correlations when using the LSM model though the average gain in skill is minimal (mean correlation skill score = 0.03). This percentage drops to 37% and 22% for improvements in skill which exceed 0.1 and 0.2

5 respectively (Fig. 8g). On the contrary, over half of stations see improvements for the KGE skill score for the hydrological model, PCR-GLOBWB and 23% of stations observe KGE skill score increases exceeding 0.25 (Fig. 8h).

A large loss in performance for the KGE can be seen when using H-TESSEL at stations in the Peruvian Amazon at the confluence point to the Solimões River with PCR-GLOBWB CaMa-Flood noting similar scores to the calibrated version of the Lisflood routing model at the San Regis (*2*) and Tamshiyacu (*4*) gauging sites (Fig. 8h). These stations have KGE skill

10 scores of -4.02 and -1.11 respectively. Model performance in this region can largely be attributed to the failure of the H-TESSEL CaMa-Flood run to accurately represent the variance of flow and the temporal correlation component of the KGE with the variability of modelled flow far higher than in the observed data (Fig. 4a). Northern regions in the Branco basin and stations situated towards the Colombian Amazon show the opposite effect with higher KGE coefficients found for the H-TESSEL CaMa-Flood run, indicating that model suitability is regionally specific.

15 **3.6 By how much does the calibration of groundwater and routing parameters improve performance?**

Calibration of hydrological models is known to be a useful tool in providing more accurate estimates of river flow (Beck et al., 2017). However, due to a lack of data and the computational expense required in the calibration of GHMs many remain uncalibrated (Bierkens, 2015; Sood & Smakhtin, 2015). To investigate the potential benefits of routing model calibration, the time series of river discharge for the calibrated Lisflood runs forced using the ERA-Interim Land and ERA-5 reanalysis

20 datasets were compared against the associated default set-ups without routing calibration. Overall, hydrological performance, on average, improves upon model parameter calibration with computed KGE skill scores for both ERA-Interim Land and ERA-5 increasing on average by 0.13 and 0.14 respectively. The influence of calibration is found to be similar between precipitation datasets with the number of stations considered skillful for the KGE upon calibration totalling 66 for both the ERA-Interim Land and ERA-5 simulations, an increase of two and four stations respectively. When observing the spatial

25 distribution of relative improvements an east/west divide can be seen (Figs. 8c & 8d). Generally, decreases in skill are concentrated to stations in the western side of the basin whereas stations located to the east display improved hydrological representation.

Three stations (*2, 3 & 4*) in the Peruvian Amazon show increased KGE skill scores when using the calibrated ERA-5 run relative to the similar uncalibrated set-up (Fig. 8d). Conversely, a loss in skill is observed at each station for the calibrated

30 run forced using ERA-Interim Land (Fig. 8c). These results are likely associated to a larger negative runoff bias within the ERA-Interim Land Lisflood_uc run relative to the ERA-5 Lisflood_uc simulation (Figs. 5c and 5e) for the three stations. This is supported by Hirpa et al. (2018) who concluded that stations which have a negative streamflow bias in the default run

(i.e. Lisflood_uc) also have a negative KGE skill score owing to the challenge of correcting a water deficit within the routing component. Thus, for GHMs which tend to underestimate runoff, adjustments of parameters within the LSM or hydrological model (e.g. those responsible for the portioning of precipitation into runoff) or through bias correction measures within the precipitation dataset may be advantageous in efforts to accurately represent floods.

5   No significant differences between calibrated and uncalibrated Lisflood correlation scores are identified between simulated and observed peaks (Fig. 7 & Table 2). In total, the number of stations exceeding the 0.6 threshold for peak flow correlations remains the same for runs involving ERA-5 and decreases by one for ERA-Interim Land meaning that the routing model calibration has very little impact on our ability to capture annual peaks with the precipitation dataset used to force the LSM more influential. This suggests that calibrated parameters controlling flow timing (e.g. Manning's channel coefficient) are

10   not as important for simulating the magnitude of higher flows in the Amazon basin and that bias correction of the precipitation or calibration of parameters associated with runoff and evapotranspiration might be more useful. As previously highlighted by Hirpa et al. (2018) the inclusion of an objective function that is explicitly based on flood peaks could improve the ability of Lisflood to simulate floods. This is supported by previous studies (Greuell et al., 2015; Beck et al., 2017) which have also identified that improved performance in calibrated models is predominately specific to metrics which are

15   incorporated into the objective function used within the calibration.

3.7 Aspects for future work

While estimating the magnitude of peak river flow is fundamental, more evaluation is required in assessing the ability to represent the timing of flood peaks. Flood peaks can occur too early in large Amazonian rivers (Alfieri et al., 2013; Hoch et al., 2017b), but accurate flow timing is of particular importance to the Amazon basin with the time displacement between

20   peak flows in coinciding tributaries a major factor in the dampening of the Amazon flood wave (Tomasella et al., 2010) and the synchronisation of peaks commonly associated with exceptional flood events throughout the Amazon basin (e.g. Marengo et al., 2012; Ovando et al., 2016).

4 Conclusions

In this paper, eight different GHMs were employed in an intercomparison analysis using two verification metrics to assess

25   model performance against gauged river discharge observations. The motivation for this work stemmed from the need to evaluate the ability of GHMs to reproduce historical floods in the Amazon basin for use in climate analysis and to identify the strengths and weaknesses which exist along the hydrological modelling chain in order to provide insight to model developers. The implications of these results suggest that the choice of precipitation dataset is the most influential component of the GHM set-up in terms of our ability to recreate annual maximum river flows in the Amazon basin. This is

30   evident with average station correlations between observed and simulated annual maximum river flows increasing when using the new ERA-5 reanalysis dataset with significant improvements in locations of the Peruvian Amazon. Although

parameter calibration of the Lisflood routing model improved the representation of the whole hydrological regime across the basin, the agreement between observed and simulated peak discharge values saw no change upon the calibration. This indicates that the benefit of calibration is confined to the objective function used, in this case the KGE, and highlights that further model calibration should be undertaken using an objective function that fits the purpose of the application (e.g.

5 RMSE of flood peaks for flood forecasting systems).

Author contributions. EZ provided data and information for all simulations incorporating Lisflood and for the ERA-Interim Land H-TESSEL CaMa-Flood set-up. ZF and JM provided data and information for the TRMM CREST EF5 and ERA-Interim Land PCR-GLOBWB CaMa-Flood runs respectively. ES, HC, JB and EC supervised the research and provided important advice. ES, HC and JT designed the analysis and JT undertook the research in addition to writing the paper. All

10 authors were involved in discussions throughout the development and commented on the manuscript.

Competing interests. The authors declare that they have no conflict of interest.

Acknowledgements. Jamie Towner is grateful for financial support from the Natural Environment Research Council (NERC) as part of the SCENARIO Doctoral Training Partnership (grant agreement NE/L002566/1). The first author is also grateful for additional travel support and funding provided by the Red Cross Red Crescent Climate Centre, to the observational and

15 national services, SO-HYBAM, SENAMHI, ANA and INAMHI for providing observed river discharge data and to the ECMWF for computer access and technical support. Finally, a specific thanks goes to Professor Christel Prudhomme and the Environmental Forecasts team in the Evaluation Section at the ECMWF for their advice and support throughout the analysis and writing of the manuscript.

References

20 Alfieri, L., Burek, P., Dutra, E., Krzeminski, B., Muraro, D., Thielen, J., and Pappenberger, F.: GloFAS-global ensemble streamflow forecasting and flood early warning, Hydrol. Earth Syst. Sci., 17, 1161, https://doi.org/10.5194/hess-17-1161-2013, 2013.

Alfieri, L., Cohen, S., Galantowicz, J., Schumann, G. J., Trigg, M. A., Zsoter, E., Prudhomme, C., Kruczkiewicz, A., Coughlan de Perez, E., Flamig, Z., Rudari., R., Wu, H., Adler, R. F., Brakenbridge, R. G., Kettner, A., Weerts, A., Matgen,

25 P., Islam, S. A. K. M., and Salamon, P.: A global network for operational flood risk reduction, Environ. Sci. Policy., 84, 149-158, https://doi.org/10.1016/j.envsci.2018.03.014, 2018.

35 Andreadis, K. M., Schumann, G. J. P., Stampoulis, D., Bates, P. D., Brakenridge, G. R., and Kettner, A. J.: Can Atmospheric Reanalysis Data Sets Be Used to Reproduce Flooding Over Large Scales?, Geophys. Res. Lett., 44, 10369-10377, https://doi.org/10.1002/2017GL075502, 2017.

Arnell, N. W., and Gosling, S. N.: The impacts of climate change on river flood risk at the global scale, Clim. Change., 134, 387-401, https://doi.org/10.1007/s10584-014-1084-5, 2016.

Arnold, J. G., Srinivasan, R., Muttiah, R. S., and Williams, J. R.: Large area hydrologic modeling and assessment part I: model development 1, J. Am. Water Resour. Assoc., 34, 73-89, 1998.

Balsamo, G., Beljaars, A., Scipal, K., Viterbo, P., van den Hurk, B., Hirschi, M., and Betts, A. K.: A revised hydrology for the ECMWF model: Verification from field site to terrestrial water storage and impact in the Integrated Forecast System, J. Hydrometeorol., 10, 623-643, https://doi.org/10.1175/2008JHM1068.1, 2009.

Balsamo, G., Pappenberger, F., Dutra, E., Viterbo, P., and Van den Hurk, B. J. J. M.: A revised land hydrology in the ECMWF model: a step towards daily water flux prediction in a fully-closed water cycle, Hydrol. Process., 25, 1046-1054, https://doi.org/10.1002/hyp.7808, 2010.

Balsamo, G., Albergel, C., Beljaars, A., Boussetta, S., Brun, E., Cloke, H.., Dee, H., Dutra, D., Muñoz-Sabater, J., Pappenberger, F., de Rosnay, P., Stockdale. T., and Vitart, F.: ERA-Interim/Land: a global land surface reanalysis data set, Hydrol. Earth Syst. Sci., 19, 389-407, https://doi.org/10.5194/hess193892015, 2015.

Beck, H. E., van Dijk, A. I., de Roo, A., Dutra, E., Fink, G., Orth, R., and Schellekens, J.: Global evaluation of runoff from ten state-of-the-art hydrological models, Hydrol. Earth Syst. Sci., 21, 2881-2903, https://doi.org/10.5194/hess-21-2881-2017, 2017.

Balsamo, G., Agusti-Panareda, A., Albergel, C., Arduini, G., Beljaars, A., Bidlot, J., Bousserez, N., Boussetta, S., Brown, A., Buizza, R., Buontempo, C., Chevallier, F., Choulga, M., Cloke, H., Cronin, M. F., Dahoui, M., De Rosnay, P., Dirmeyer, P. A., Drusch, M., Dutra, E., Ek, M. B., Gentine, P., Hewitt, H., Keeley, S. P. E., Kerr, Y., Kumar, S., Lupu, C., Mahfouf, J. F., McNorton, J., Mecklenburg, S., Mogensen, K., Muñoz-Sabater, J., Orth, R., Rabier, F., Reichle, R., Ruston, B, Pappenberger, F., Sandu, I., Seneviratne, S. I., Tietsche, S., Trigo, I. F., Uijlenhoet, R., Wedi, N., Woolway, R. L., & Zeng, X.: Satellite and In Situ Observations for Advancing Global Earth Surface Modelling: A Review. Remote Sens., 10, 2038, https://doi.org/10.3390/rs10122038, 2018.

Beven, K. J.: *Rainfall-Runoff Modelling: The Primer*, 2nd ed., Wiley-Blackwell, Chichester, U.K, 2012.

Bierkens, M. F.: Global hydrology 2015: State, trends, and directions, Water Resour. Res., 51, 4923-4947., https://doi.org/10.1002/2015WR017173, 2015.

Bierkens, M. F., Bell, V. A., Burek, P., Chaney, N., Condon, L. E., David, C. H., de Roo, A., Döll, P., Drost, N., Famigiletti, J.S., Flörke, M., Gochis, D. J., Houser, P., Hut, R., Keune, J., Kollet, S., Maxwell, R. M., Reager, J. T., Samaniego, L., Sudicky, E., Sutanudiaia, E. H., van de Giesen, N., Winsemius, H., and Wood, E. F.: Hyper-resolution global hydrological modelling: what is next? "Everywhere and locally relevant", Hydrol. Process., 29, 310-320, https://doi.org/10.1002/hyp.10391, 2015.

Bondeau, A., Smith, P. C., Zaehle, S., Schaphoff, S., Lucht, W., Cramer, W., Gerten, D., Lotze-Campen, H., Muller, C., ̈ Reichstein, M., and Smith, B.: Modelling the role of agriculture for the 20th century global terrestrial carbon balance, Global Change Biol., 13, 679–706, https://doi.org/10.1111/j.1365- 2486.2006.01305.x, 2007.

Butts, M. B., Payne, J. T., Kristensen, M., and Madsen, H.: An evaluation of the impact of model structure on hydrological modelling uncertainty for streamflow simulation, J. Hydrol., 298, 242-266, https://doi.org/10.1016/j.jhydrol.2004.03.042, 2004.

Clark III, R. A., Flamig, Z. L., Vergara, H., Hong, Y., Gourley, J. J., Mandl, D. J., Frye, S., Handy, M., and Patterson, M.:
5 Hydrological modeling and capacity building in the Republic of Namibia, Bull. Am. Meteorol. Soc., 98, 1697-1715, https://doi.org/10.1175/BAMS-D-15-00130.1, 2016.

Correa, S. W., de Paiva, R. C. D., Espinoza, J. C., and Collischonn, W.: Multi-decadal Hydrological Retrospective: Case study of Amazon floods and droughts, J. Hydrol., 549, 667-684, https://doi.org/10.1016/j.jhydrol.2017.04.019, 2017.

Coughlan de Perez, E., van den Hurk, B. J. J. M., Van Aalst, M. K., Jongman, B., Klose, T., and Suarez, P.: Forecast-based
10 financing: an approach for catalyzing humanitarian action based on extreme weather and climate forecasts, Nat. Hazards Earth Syst. Sci., 15, 895-904, https://doi.org//10.5194/nhess-15-895-2015, 2015.

De Groeve, T., Thielen-del Pozo, J., Brakenridge, R., Adler, R., Alfieri, L., Kull, D., Lindsay, F., Imperiali, O., Pappenberger, F., Rudari, R., Salamon, P., Villars, N., and Wyjad, K.: Joining forces in a global flood partnership, Bull. Am. Meteorol. Soc., 96, ES97-ES100, https://doi.org/10.1175/BAMS-D-14-00147.1, 2015.

15 Dee, D. P., Uppala, S. M., Simmons, A. J., Berrisford, P., Poli, P., Kobayashi, S., Andrae, U., Balmaseda, M.A., Balsamo, G., Bauer, P., Bechtold, P., Belijaars, A.C.M., van de Berg, L., Bidlot, J., Bormann, N., Delsol, C., Dragani, R., Fuentes, M., Geer, A.J., Haimberger, L., Healy, S.B., Hersbach, S., Hólm, E.V., Isaksen, L., Kallberg, P., Köhler, M, Matricardi, M., McNally, A.P., Mong-Sanz, B.M., Morcrette, J.J., Park, B.K., Peubey, C., de Rosnay, P., Tavolato, C., Thèpaut, J.N., and Vitart, F.: The ERA-Interim reanalysis: Configuration and performance of the data assimilation system, Q. J. R. Meteorol.
20 Soc., 137, 553-597, https://doi.org/10.1002/qj.828, 2011.

Devia, G. K., Ganasri, B. P., & Dwarakish, G. S.: A review on hydrological models, Aquatic Procedia., 4, 1001-1007., https://doi.org/10.1016/j.aqpro.2015.02.126, 2015.

Döll, P., Kaspar, F., and Lehner, B.: A global hydrological model for deriving water availability indicators: model tuning and validation, J. Hydrol., 270, 105-134, https://doi.org/10.1016/S0022-1694(02)00283-4, 2003.

25 ECMWF.: A brief description of reforecasts: https://confluence.ecmwf.int/display/S2S/A+brief+description+of+reforecasts, last access: 25 September 2018, 2016.

ECMWF.: What are the changes from ERA-Interim to ERA5?:
https://confluence.ecmwf.int//pages/viewpage.action?pageId=74764925, Last access: 31st August 2018, 2017.

ECMWF.: What is ERA-5?: https://confluence.ecmwf.int/display/CKB/What+is+ERA5, last access: 8 October 2018.

30 Emerton, R. E., Stephens, E. M., Pappenberger, F., Pagano, T. C., Weerts, A. H., Wood, A. W., Salamon, P., Brown, J. D., Hierdt, N., Donnelly, C., Baughc C. A., and Cloke, H. L.: Continental and global scale flood forecasting systems, Wiley Interdiscip. Rev. Water, 3, 391-418, https://doi.org/10.1002/wat2.1137, 2016.

Emerton, R., Zsoter, E., Arnal, L., Cloke, H. L., Muraro, D., Prudhomme, C., Stephens, E.M., Salamon, P., and Pappenberger, F.: Developing a global operational seasonal hydro-meteorological forecasting system: GloFAS v2. 2 Seasonal v1. 0, Geosci. Model Dev., 11, 3327-3346, https://doi.org/10.5194/gmd-11-3327-2018, 2018.

Espinoza, J. C., Ronchail, J., Guyot, J. L., Cochonneau, G., Naziano, F., Lavado, W., De Oliveria, E., Pombosa, R., and Vauchel, P.: Spatio-temporal rainfall variability in the Amazon basin countries (Brazil, Peru, Bolivia, Colombia, and Ecuador), Int. J. Climatol., 29, 1574-1594, https://doi.org/10.1002/joc.1791, 2009.

Espinoza, J. C., Ronchail, J., Frappart, F., Lavado, W., Santini, W., and Guyot, J. L.: The major floods in the Amazonas River and tributaries (western Amazon basin) during the 1970–2012 period: A focus on the 2012 flood, J. Hydrometeorol., 14, 1000-1008, https://doi.org/10.1175/JHM-D-12-0100.1, 2013.

Espinoza, J. C., Marengo, J. A., Ronchail, J., Carpio, J. M., Flores, L. N., and Guyot, J. L.: The extreme 2014 flood in south-western Amazon basin: the role of tropical-subtropical South Atlantic SST gradient, Environ. Res. Lett., 9, 124007, https://doi.org/10.1088/1748-9326/9/12/124007, 2014.

Espinoza, J. C., Ronchail, J., Marengo, J. A., and Segura, H.: Contrasting North–South changes in Amazon wet-day and dry-day frequency and related atmospheric features (1981–2017), Clim. Dyn., 1-18, https://doi.org/10.1007/s00382-018-4462-2, 2018.

Forbes, R., Haiden, T., and Magnusson, L.: Improvements in IFS forecasts of heavy precipitation. Meteorology section of ECMWF newsletter No. 144., 21-26, https://doi.org/10.21957/jxtonky0, 2015.

Gilleland, M. E.: Package 'verification', http://cran.utstat.utoronto.ca/web/packages/verification/verification.pdf, last access 25 September 2018, 2015.

Gloor, M. R. J. W., Brienen, R. J., Galbraith, D., Feldpausch, T. R., Schöngart, J., Guyot, J. L., Espinoza, J. C., Llyod, J., and Phillips, O. L.: Intensification of the Amazon hydrological cycle over the last two decades, Geophys. Res. Lett., 40, 1729-1733, https://doi.org/10.1002/grl.50377, 2013.

Gosling, S. N., and Arnell, N. W.: Simulating current global river runoff with a global hydrological model: model revisions, validation, and sensitivity analysis, Hydrol. Processes, 25, 1129-1145, https://doi.org/10.1002/hyp.7727, 2011.

Gourley, J. J., Flamig, Z. L., Vergara, H., Kirstetter, P. E., Clark III, R. A., Argyle, E., Arthur, A., Martinaitis, S., Terti, G., Erlingis, J.M., Hong, Y., and Howard, K.W.: The FLASH Project: Improving the tools for flash flood monitoring and prediction across the United States, Bull. Am. Meteorol. Soc., 98, 361-372, https://doi.org/10.1175/BAMS-D-15-00247.1, 2017.

Greuell, J. W., Andersson, J., Donnelly, C., Feyen, L., Gerten, D., Ludwig, F., Pisacane, G., Roudier, P., and Schaphoff, S.: Evaluation of five hydrological models across Europe and their suitability for making projections under climate change Hydrol. Earth Syst. Sci. Discuss.12, 10289-10330, https://doi.org/10.5194/hessd-12-10289-2015, 2015.

Gudmundsson, L., Wagener, T., Tallaksen, L.M., and Engeland, K.: Evaluation of nine large-scale hydrological models with respect to the seasonal runoff climatology in Europe, Water Resour. Res., 48, https://doi.org/10.1029/2011WR010911, 2012.

Gupta, H. V., Kling, H., Yilmaz, K. K., and Martinez, G. F.: Decomposition of the mean squared error and NSE performance criteria: Implications for improving hydrological modelling , J. Hydrol., 377, 80-91, https://doi.org/10.1016/j.jhydrol.2009.08.003, 2009.

Guse, B., Pfannerstill, M., Gafurov, A., Kiesel, J., Lehr, C., and Fohrer, N.: Identifying the connective strength between model parameters and performance criteria, Hydrol. Earth Syst. Sci., 21, 5663-5679, https://doi.org/10.5194/hess-21-5663-2017, 2017.

Haddeland, I., Clark, D. B., Franssen, W., Ludwig, F., VOß, F., Arnell, N. W., Bertrand, N., Best, M., Folwell, S., Gerten, D., Gomes, S., Gosling, S.N., Hagemann, S., Hanasaki, N., Harding, R., Heinke, J., Kabat, P., Koirala, S, Oki, T., Polcher, J., Stacke, T., Viterbo, P., Weedon, G.P., and Yeh, P.: Multimodel estimate of the global terrestrial water balance: Setup and first results, J. Hydrometeorol., 12, 869-884, https://doi.org/10.1175/2011JHM1324.1, 2011.

Hattermann, F. F., Krysanova, V., Gosling, S. N., Dankers, R., Daggupati, P., Donnelly, C., Flörke, M., Huang, S., Motovilov, Y., Buda, S., Yang, T., Müller, C., Leng, G., Tang, Q., Portmann, F. T., Hagemann, S., Gerten, D., Wada, Y., Masaki, Y., Alemayehu, T., Satoh, Y., and Samaniego, L.: Cross-scale intercomparison of climate change impacts simulated by regional and global hydrological models in eleven large river basins, J. Clim. Change, 141, 561-576, https://doi.org/10.1007/s10584-016-1829-4, 2017.

Hirabayashi, Y., Mahendran, R., Koirala, S., Konoshima, L., Yamazaki, D., Watanabe, S., Kim, H., and Kanae, S.: Global flood risk under climate change, Nat. Clim. Chang., 3, 816, https://doi.org/10.1038/nclimate1911, 2013.

Hirpa, F. A., Salamon, P., Beck, H. E., Lorini, V., Alfieri, L., Zsoter, E., and Dadson, S. J.: Calibration of the Global Flood Awareness System (GloFAS) using daily streamflow data, J. Hydrol., 566, 595-606, https://doi.org/10.1016/j.jhydrol.2018.09.052, 2018.

Hoch, J. M., Haag, A. V., Dam, A. V., Winsemius, H. C., van Beek, L. P., and Bierkens, M. F.: Assessing the impact of hydrodynamics on large-scale flood wave propagation–a case study for the Amazon Basin, Hydrol. Earth Syst. Sci., 21, 117-132, https://doi.org/10.5194/hess-21-117-2017, 2017a.

Hoch, J. M., Neal, J., Baart, F., van Beek, L. P. H., Winsemius, H., Bates, P., and Bierkens, M. F.: GLOFRIM v1. 0–A globally applicable computational framework for integrated hydrological–hydrodynamic modelling, Geosci. Model Dev., 10, 3913-3929, https://doi.org/10.5194/gmd-10-3913-2017, 2017b.

Huffman, G. J., Bolvin, D. T., Nelkin, E. J., Wolff, D. B., Adler, R. F., Gu, G., Hong, Y., Bowman, K.P., and Stocker, E. F.: The TRMM multisatellite precipitation analysis (TMPA): Quasi-global, multiyear, combined-sensor precipitation estimates at fine scales, J. Hydrometeorol., 8, 38-55, https://doi.org/10.1175/JHM560.1, 2007.

Huffman, G. J., Adler, R. F., Bolvin, D. T., and Gu, G.: Improving the global precipitation record: GPCP version 2.1, Geophys. Res. Lett., 36, https://doi.org/10.1029/2009GL040000, 2009.

IFRC.: Disaster Relief Fund (DREF) Peru: Floods. https://reliefweb.int/sites/reliefweb.int/files/resources/MDRPE005du1.pdf, last access: 25 September 2018, 2013.

Kling, H., Fuchs, M., and Paulin, M.: Runoff conditions in the upper Danube basin under an ensemble of climate change scenarios, J. Hydrol., 424, 264-277, https://doi.org/10.1016/j.jhydrol.2012.01.011, 2012.

Latrubesse, E. M., Arima, E. Y., Dunne, T., Park, E., Baker, V. R., d'Horta, F. M., Wight, C., Wittmann, F., Zuanon, J., Baker, P. A., Ribas, C. C., Norgaard, R. B., Filizola, N., Ansar, A., Flyvbjerg, B., and Stevaux, J. C.: Damming the rivers of the Amazon basin. Nature, 546, 363, https://doi.org/10.1038/nature22333, 2017.

Legates, D. R., and McCabe, G. J.: Evaluating the use of "goodness-of-fit" measures in hydrologic and hydroclimatic model validation, Water Resour. Res., 35, 233-241, https://doi.org/10.1029/1998WR900018, 1999.

Lehner, B., Verdin, K., and Jarvis, A.: New global hydrography derived from spaceborne elevation data. Eos, Transactions American Geophysical Union, 89, 93-94, https://doi.org/200810.1029/2008EO100001, 2008.

Magilligan, F. J., and Nislow, K. H.: Changes in hydrologic regime by dams. Geomorphology, 71, 61-78, https://doi.org/10.1016/j.geomorph.2004.08.017, 2005.

Marengo, J. A., Tomasella, J., Soares, W. R., Alves, L. M., and Nobre, C. A.: Extreme climatic events in the Amazon basin, Theor. Appl. Climatol., 107, 73-85, https://doi.org/10.1007/s00704-011-0465-1, 2012.

Marengo, J. A., Alves, L. M., Soares, W. R., Rodriguez, D. A., Camargo, H., Riveros, M. P., and Pabló, A. D.: Two contrasting severe seasonal extremes in tropical South America in 2012: flood in Amazonia and drought in northeast Brazil, J. Clim., 26, 9137-9154, https://doi.org/10.1175/JCLI-D-12-00642.1, 2014.

Marengo, J. A., and Espinoza, J. C.: Extreme seasonal droughts and floods in Amazonia: causes, trends and impacts, Int. J. Climatol., 36, 1033-1050, https://doi.org/10.1002/joc.4420, 2015.

Meade, R. H., Rayol, J. M., Da Conceicão, S. C., and Natividade, J. R.: Backwater effects in the Amazon River basin of Brazil, Environ. Geol. Water Sci., 18, 105-114, https://doi.org/10.1007/BF01704664, 1991.

Meigh, J. R., McKenzie, A. A., and Sene, K. J.: A grid-based approach to water scarcity estimates for eastern and southern Africa, Water Resour. Mange., 13, 85-115, https://doi.org/10.1023/A:1008025703712, 1999.

Meng, J., Li, L., Hao, Z., Wang, J., and Shao, Q.: Suitability of TRMM satellite rainfall in driving a distributed hydrological model in the source region of Yellow River, J. Hydrol., 509, 320-332, https://doi.org/10.1016/j.jhydrol.2013.11.049, 2013.

Mittermaier, M., Roberts, N., and Thompson, S. A.: A long-term assessment of precipitation forecast skill using the Fractions Skill Score, Meterol. Appl., 20, 176-186, https://doi.org/10.1002/met.296, 2013.

Mundial Grupo Banco: http://bibliotecadigital.planejamento.gov.br/xmlui/bitstream/handle/iditem/658/Banco%20Mundial_opcoes_de%20prote%C3%A7%C3%A3o%20financeira%20contra%20desastres%20no%20Brasil.pdf?sequence=1, last Access: 25 September 2018, 2014.

Nash, J. E., and Sutcliffe, J. V.: River flow forecasting through conceptual models part I—A discussion of principles , J. Hydrol., 10, 282-290, https://doi.org/10.1016/0022-1694(70)90255-6, 1970.

Novak, D. R., Bailey, C., Brill, K. F., Burke, P., Hogsett, W. A., Rausch, R., and Schichtel, M.: Precipitation and temperature forecast performance at the Weather Prediction Center, Weather Forecasting, 29, 489-504, https://doi.org/10.1175/WAF-D-13-00066.1, 2014.

Ovando, A., Tomasella, J., Rodriguez, D. A., Martinez, J. M., Siqueira-Junior, J. L., Pinto, G. L. N., Passy, P., Vauchel, P,

5   Noriega, L., and von Randow, C.: Extreme flood events in the Bolivian Amazon wetlands., J. Hydrol.: Reg. Stud., 5, 293-308, https://doi.org/10.1016/j.ejrh.2015.11.004, 2016.

Paiva, R. C. D., Buarque, D. C., Collischonn, W., Bonnet, M. P., Frappart, F., Calmant, S., and Mendes, C. A. B.: Large-scale hydrologic and hydrodynamic modeling of the Amazon River basin, Water Resour. Res., 49, 1226-1243, https://doi.org/10.1002/wrcr.20067, 2013.

10   Pappenberger, F., Dutra, E., Wetterhall, F., and Cloke, H. L.: Deriving global flood hazard maps of fluvial floods through a physical model cascade, Hydrol. Earth Syst. Sci., 16, 4143-4156, https://doi.org/10.5194/hess-16-4143-2012, 2012.

Revilla-Romero, B., Beck, H. E., Burek, P., Salamon, P., de Roo, A., and Thielen, J.: Filling the gaps: Calibrating a rainfall-runoff model using satellite-derived surface water extent, Remote Sens. Environ., 171, 118-131, https://doi.org/10.1016/j.rse.2015.10.022, 2015.

15   Ronchail, J., Cochonneau, G., Molinier, M., Guyot, J. L., Chaves, A. G. D. M., Guimarães, V., and De Oliveira, E.: Interannual rainfall variability in the Amazon basin and sea-surface temperatures in the equatorial Pacific and the tropical Atlantic Oceans, Int. J. Climatol., 22, 1663-1686, https://doi.org/10.1002/joc.815, 2002.

Sampson, C. C., Smith, A. M., Bates, P. D., Neal, J. C., Alfieri, L., and Freer, J. E.: A high-resolution global flood hazard model, Water Resour. Res., 51, 7358-7381, https://doi.org/10.1002/2015WR016954, 2015.

20   Schöngart, J., and Junk, W. J.: Forecasting the flood-pulse in Central Amazonia by ENSO-indices, J. Hydrol., 335, 124-132, https://doi.org/10.1016/j.jhydrol.2006.11.005, 2007.

Smith, P., Pappenberger, F., Wetterhall, F., Thielen, J., Krzeminski, B., Salamon, P., Muraro, D., Kalas, M., and Baugh, C.: On the operational implementation of the European Flood Awareness System (EFAS), ECMWF Tech. Memorandum, 778, 1–34, 2016.

25   Sood, A., and Smakhtin, V.: Global hydrological models: a review, Hydrol. Sci. J., 60, 549-565, https://doi.org/10.1080/02626667.2014.950580, 2015.

Sutanudjaja, E. H., Beek, R. V., Wanders, N., Wada, Y., Bosmans, J. H., Drost, van der Ent, R. J., de Graaf, I. E. M., Hoch, J. M., de Jong, K., Karssenberg, D., López López, P., Peßenteiner, S., Schmitz, O., Straatsma, M. W., Vannametee, E., Wisser, D., and Bierkens, M. F. P., N.: PCR-GLOBWB 2: a 5 arcmin global hydrological and water resources model,

30   Geosci. Model Dev., 11, 2429-2453, https://doi.org/10.5194/gmd-11-2429-2018, 2018.

Timpe, K., and Kaplan, D.: The changing hydrology of a dammed Amazon, Sci. Adv. 3, e1700611, https://doi.org/10.1126/sciadv.1700611, 2017.

Tomasella, J., Borma, L. S., Marengo, J. A., Rodriguez, D. A., Cuartas, L. A., A. Nobre, C., and Prado, M. C.: The droughts of 1996–1997 and 2004–2005 in Amazonia: hydrological response in the river main-stem, Hydrol. Processes, 25, 1228-1242, https://doi.org/10.1002/hyp.7889, 2010.

Trigg, M. A., Birch, C. E., Neal, J. C., Bates, P. D., Smith, A., Sampson, C. C., Yamazaki, D., Hirabayashi, Y., Pappenberger, F., Dutra, E., Ward, P. J., Winsemius, H. C., Salamon, P., Dottorri, F., Rudari, R., Kappes, M. S., Simpson, A. L., Hadzilacos, G., and Fewtrell, T. J.: The credibility challenge for global fluvial flood risk analysis, Environ. Res. Lett., 11, 094014, https://doi.org/10.1088/1748-9326/11/9/094014, 2016.

van Beek, L. P. H. and Bierkens, M. F. P.: The Global Hydrological Model PCR-GLOBWB: Conceptualization, Parameterization and Verification, available at: http://vanbeek.geo.uu. nl/suppinfo/vanbeekbierkens2009.pdf (last access: 03 September 2018), 2008.

van Beek, L. P. H., Wada, Y., and Bierkens, M. F. P.: Global monthly water stress: 1. Water balance and water availability, Water Resour. Res., 47, W07517, https://doi.org/10.1029/2010WR009791, 2011.

van den Hurk, B. J. J. M., Viterbo, P., Beljaars, A. C. M., and Betts, A. K.: Offline validation of the ERA40 surface scheme, ECMWF TechMemo 295, Reading, UK, 2000.

van den Hurk, B. J., and Viterbo, P.: The Torne-Kalix PILPS 2 (e) experiment as a test bed for modifications to the ECMWF land surface scheme, Glob. Planet. Chang., 38, 165-173, https://doi.org/10.1016/S0921-8181(03)00027-4, 2003.

van Der Knijff, J. M., Younis, J., and De Roo, A. P. J.: LISFLOOD: a GIS-based distributed model for river basin scale water balance and flood simulation, Int. J. Geogr. Inf. Sci., 24, 189-212, https://doi.org/10.1080/13658810802549154, 2010.

van Huijgevoort, M. H. J., Van Lanen, H. A. J., Teuling, A. J., and Uijlenhoet, R.: Identification of changes in hydrological drought characteristics from a multi-GCM driven ensemble constrained by observed discharge, J. Hydrol., 512, 421-434., https://doi.org/10.1016/j.jhydrol.2014.02.060, 2014.

Wang, J., Hong, Y., Li, L., Gourley, J. J., Khan, S. I., Yilmaz, K. K., Adler, R.F., Policelli, F.S., Habib, S., Irwn, D., Limaye, A. S., Korme, T., and Okello, L.: The coupled routing and excess storage (CREST) distributed hydrological model, Hydrol. Sci. J., 56, 84-98, https://doi.org/10.1080/02626667.2010.543087, 2011.

Ward, P. J., Jongman, B., Salamon, P., Simpson, A., Bates, P., De Groeve, T., Muis, S., Coughlan de Perez, E., Rudari, R., Trigg, M. A., and Winsemius, H. C.: Usefulness and limitations of global flood risk models, Nat. Clim. Chang., 5, 712-715, https://doi.org/10.1038/nclimate2742, 2015.

Werner, M., Schellekens, J., Gijsbers, P., van Dijk, M., van den Akker, O., and Heynert, K.: The Delft-FEWS flow forecasting system, Environ. Model. Softw., 40, 65-77, https://doi.org/10.1016/j.envsoft.2012.07.010, 2013.

Wood, E. F., Roundy, J. K., Troy, T. J., Van Beek, L. P. H., Bierkens, M. F., Blyth, E., Roo, D.A., Döll, P., Ek, M., Famigiletti, J., Gochish, D., van de Giesen, N., Houser, P., Jaffé, P.R., Kollet, S., Lehner, B., Lettenmaier, D.P., Peters-Lidard, C., Sivapalan, M, Sheffield, J., Wade, A., and Whitehead, P.: Hyperresolution global land surface modeling: Meeting a grand challenge for monitoring Earth's terrestrial water, Water Resour. Res., 47, https://doi.org/10.1029/2010WR010090, 2011.

Xue, X., Hong, Y., Limaye, A., Gourley, J., Huffman, G., Khan, S., Dorji, C., and Chen, S.: Statistical and hydrological evaluation of TRMM-based Multi-Satellite Precipitation Analysis over the Wangchu Basin of Bhutan: Are the latest satellite precipitation products 3B42V7 ready for use in ungauged basins?, J. Hydrol., 499, 91–99, http s://doi.org/10.1016/j .jhydrol.2013.06.042, 2013.

5 Yamazaki, D., Kanae, S., Kim, H., and Oki, T.: A physically based description of floodplain inundation dynamics in a global river routing model, Water Resour. Res., 47, https://doi.org/10.1029/2010WR009726, 2011.

Yamazaki, D., Lee, H., Alsdorf, D. E., Dutra, E., Kim, H., Kanae, S., and Oki, T.: Analysis of the water level dynamics simulated by a global river model: A case study in the Amazon River, Water Resour. Res., 48, https://doi.org/10.1029/2012WR011869, 2012.

10 Yamazaki, D., O'Loughlin, F., Trigg, M. A., Miller, Z. F., Pavelsky, T. M., and Bates, P. D.: Development of the global width database for large rivers, Water Resour. Res., 50, 3467-3480., https://doi.org/10.1002/2013WR014664, 2014a.

Yamazaki, D., Sato, T., Kanae, S., Hirabayashi, Y., and Bates, P. D.: Regional flood dynamics in a bifurcating mega delta simulated in a global river model, Geophys. Res. Lett., 41, 3127-3135, https://doi.org/10.1002/2014GL059744, 2014b.

Zambrano-Bigiarini, M.: Package 'hydroGOF. Goodness-of-fit Functions for Comparison of Simulated and Observed

15 Hydrological Time Series, http://www.rforge.net/hydroGOF/, last access: 25 September 2018, 2017.

Zhang, Y., Hong, Y., Wang, X., Gourley, J. J., Xue, X., Saharia, M., Ni, G., Wang, G., Huang, Y., Chen, S., and Tang, G.: Hydrometeorological analysis and remote sensing of extremes: Was the July 2012 Beijing flood event detectable and predictable by global satellite observing and global weather modeling systems? J. Hydrometeor., 16, 381-395, https://doi.org/10.1175/JHM-D-14-0048.1, 2015.

20 Zhang, Y., Zheng, H., Chiew, F. H., Arancibia, J. P., and Zhou, X.: Evaluating regional and global hydrological models against streamflow and evapotranspiration measurements, J. Hydrometeorol., 17, 995-1010, https://doi.org/10.1175/JHM-D-15-0107.1, 2016.

Zhao, F., Veldkamp, T. I., Frieler, K., Schewe, J., Ostberg, S., Willner, S., Schauberger, B., Gosling, S. N., Schmied, H. M., Portmann, F. T., Leng, G., Huang, M., Liu, X., Tang, Q., Hanasaki, N., Biemans, H., Gerten, D., Satoh, Y., Pkhrel, Y.,

25 Stacke, T., Ciais, P., Chang, J., Ducharne, A., Guimberteau, M., Wada, Y, Kim, H., and Yamazaki, D.: The critical role of the routing scheme in simulating peak river discharge in global hydrological models, Environ. Res. Lett., 12, 075003, https://doi.org/10.1088/1748-9326/aa7250, 2017.

Zsoter, E., Cloke, H., Stephens, E., de Rosnay, P., Muñoz-Sabater, J., Prudhomme, C., and Pappenberger, F.: How well do operational Numerical Weather Prediction setups represent hydrology?., J. Hydrometeorol., in review, 2018.
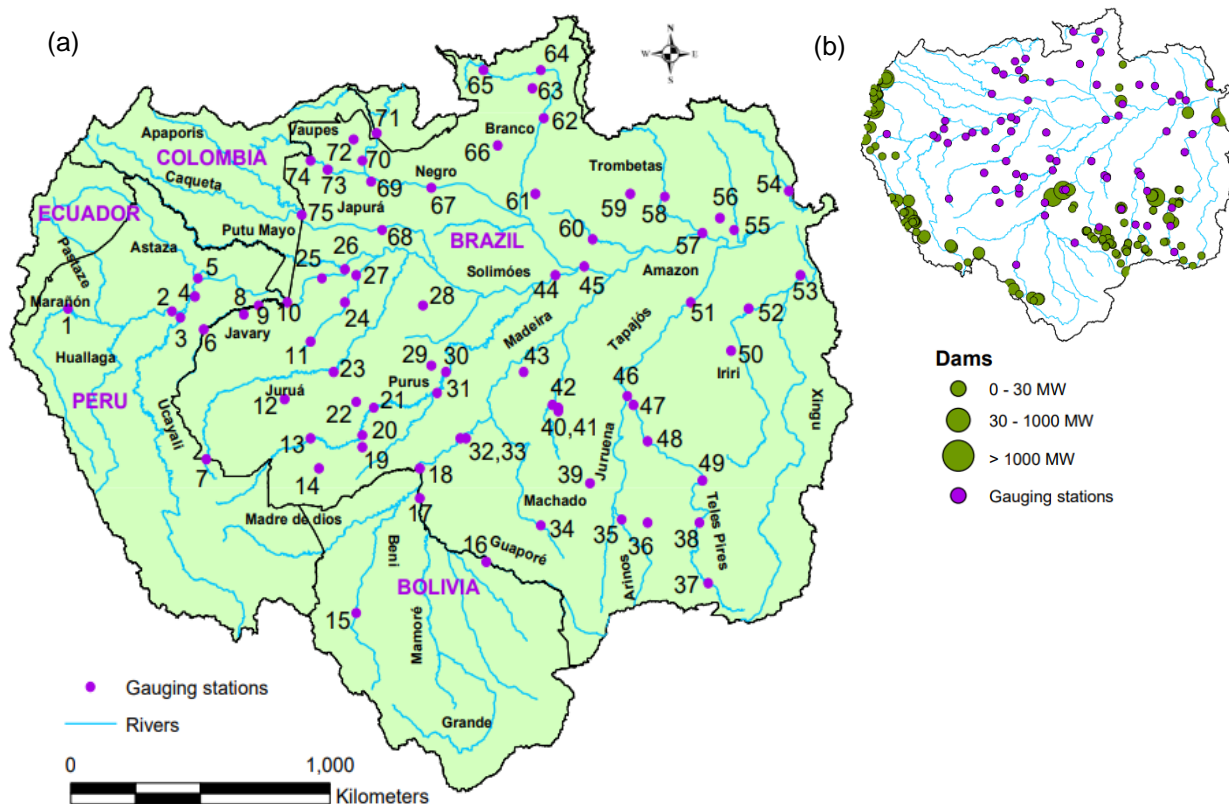
Figure 1: (a) Locations of the 75 hydrological gauges and the river network of the Amazon basin. Numbers represent stations which are referred to throughout the main text in italics. For station information see Table S1. (b) Locations of existing and under-construction dams as of 2017 (see Latrubesse et al., 2017).

5 **Table 1: Characteristics of the eight GHMs used to produce estimates of daily discharge.**

Model Run	Meteorological forcing[1]	GHM[2]	GHM Spatial Resolution	Routing Model[3]	Routing Spatial Resolution	Temporal Resolution	Start	End	Calibration	Authors
ERA-I Land H-TESSEL Lisflood_uc	ERA-I Land	H-TESSEL	~0.75^0 (~80 km)	Lisflood	0.10^0 (~10 km)	Daily	01 Jan 1997	31 Dec 2015	None	Balsamo et al. (2015)[1] Balsamo et al. (2009)[2] van der Knijff et al. (2010)[3]
ERA-I Land H-TESSEL Lisflood_c	ERA-I Land	H-TESSEL	~0.75^0 (~80 km)	Lisflood	0.10^0 (~10 km)	Daily	01 Jan 1997	31 Dec 2015	See Hirpa et al. (2018)	Balsamo et al. (2015)[1] Balsamo et al. (2009)[2] van der Knijff et al. (2010)[3]
ERA-5 H-TESSEL Lisflood_uc	ERA-5	H-TESSEL	~0.28^0 (~31 km)	Lisflood	0.10^0 (~10 km)	Daily	01 Jan 1997	31 Dec 2015	None	See ECMWF (2018)[1] Balsamo et al. (2009)[2] van der Knijff et al. (2010)[3]
ERA-5 Lisflood H-TESSEL_c	ERA-5	H-TESSEL	~0.28^0 (~31 km)	Lisflood	0.10^0 (~10 km)	Daily	01 Jan 1997	31 Dec 2015	See Hirpa et al. (2018)	See ECMWF (2018)[1] Balsamo et al. (2009)[2] van der Knijff et al. (2010)[3]
Reforecasts H-TESSEL Lisflood_c	ECMWF 20-year control Reforecasts	H-TESSEL	~0.28^0 (~31 km)	Lisflood	0.10^0 (~10 km)	Daily	01 Jan 1997	31 Dec 2015	See Hirpa et al. (2018)	See ECMWF (2017)[1] Balsamo et al. (2009)[2] van der Knijff et al. (2010)[3]
ERA-I Land H-TESSEL CaMa-Flood	ERA-I Land	H-TESSEL	~0.75^0 (~80 km)	CaMa-Flood	0.25^0 (~25 km)	Daily	01 Jan 1997	31 Dec 2015	None	Balsamo et al. (2015)[1] Balsamo et al. (2009)[2] Yamazaki et al. (2011)[3]
ERA-I Land PCR-GLOBWB CaMa-Flood	ERA-I Land	PCR-GLOBWB	~0.50^0 (~50 km)	CaMa-Flood	0.25^0 (~25 km)	Daily	01 Jan 1997	31 Dec 2015	None	Balsamo et al. (2015)[1] Sutanudjaja et al. (2018)[2] Yamazaki et al. (2011)[3]
TRMM CRESTEF5	TMPA 3B42 v7. Real-time	EF5/CREST	~0.25^0 (~25 km)	EF5/CREST	0.05^0 (~5 km)	Daily	01 Jan 2003	31 Dec 2015	None	Huffman et al. (2007)[1] Wang et al. (2011)[2] Clark et al. (2016)[3]
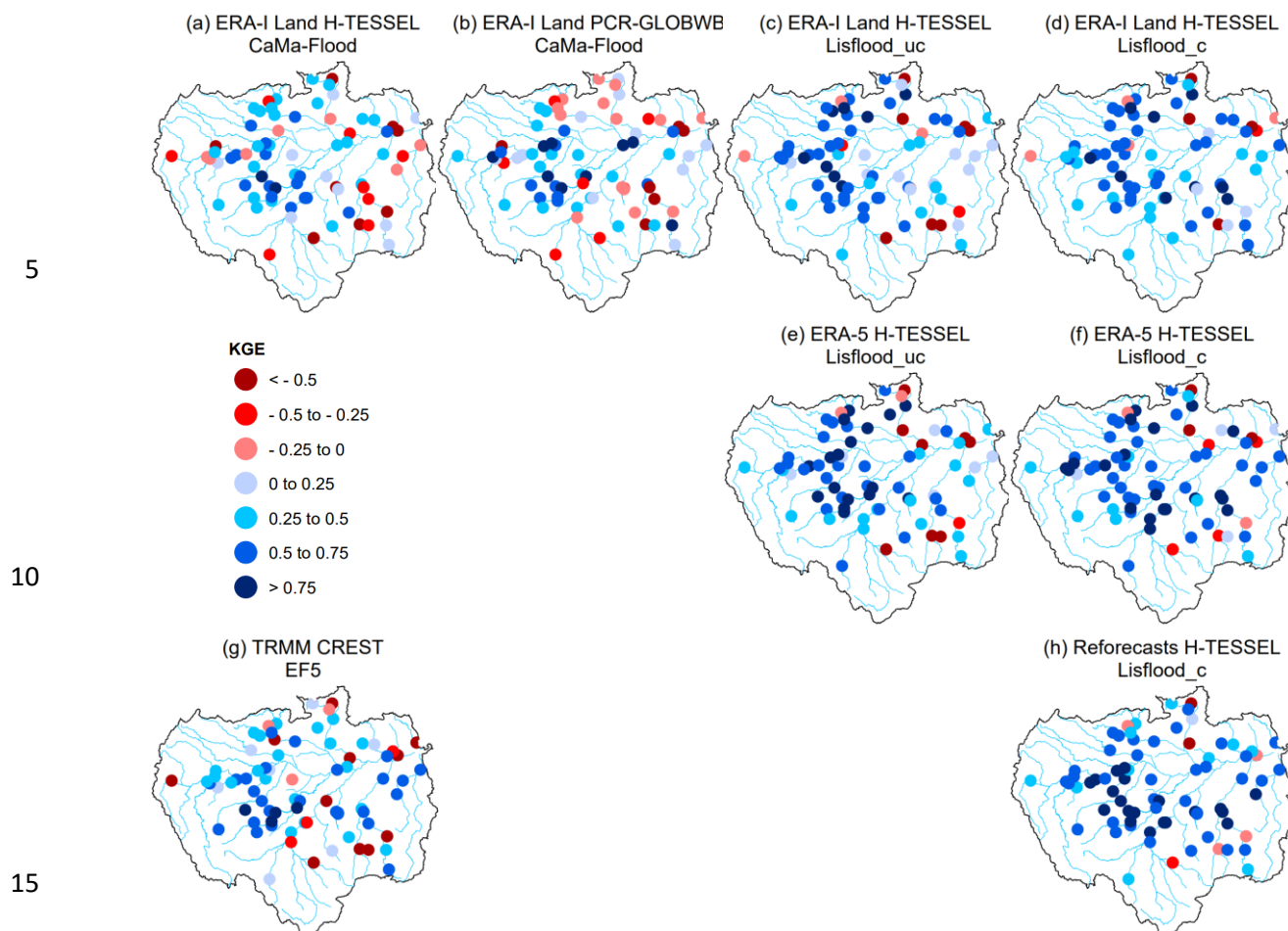
Figure 2: Full KGE scores at 75 hydrological gauging stations for all simulations for the period 1997-2015 and 2004-2015 for CREST EF5 (g). Values greater than zero are considered skilful (i.e. blue circles). To allow for easier model comparisons, plots are arranged by the different precipitation datasets (rows) and routing models (columns) with the exception of EF5 (g). For example, the final column consists of model runs using the calibrated Lisflood routing model.
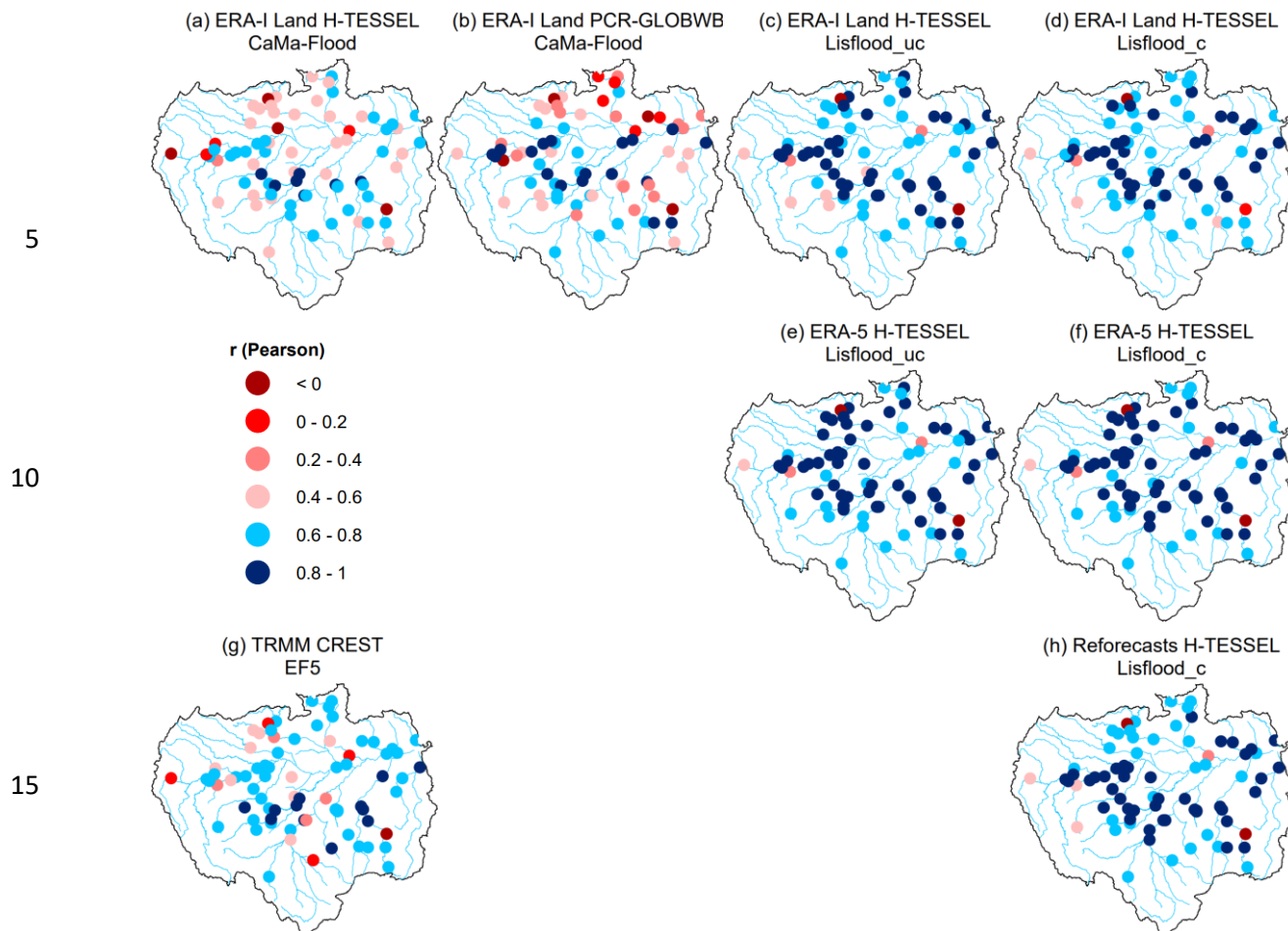
Figure 3: Correlation component of the KGE (Pearson's) at 75 hydrological gauging stations for all simulations for the period 1997-2015 and 2004-2015 for CREST EF5 (g). Values greater than 0.6 are considered skilful (i.e. blue circles).
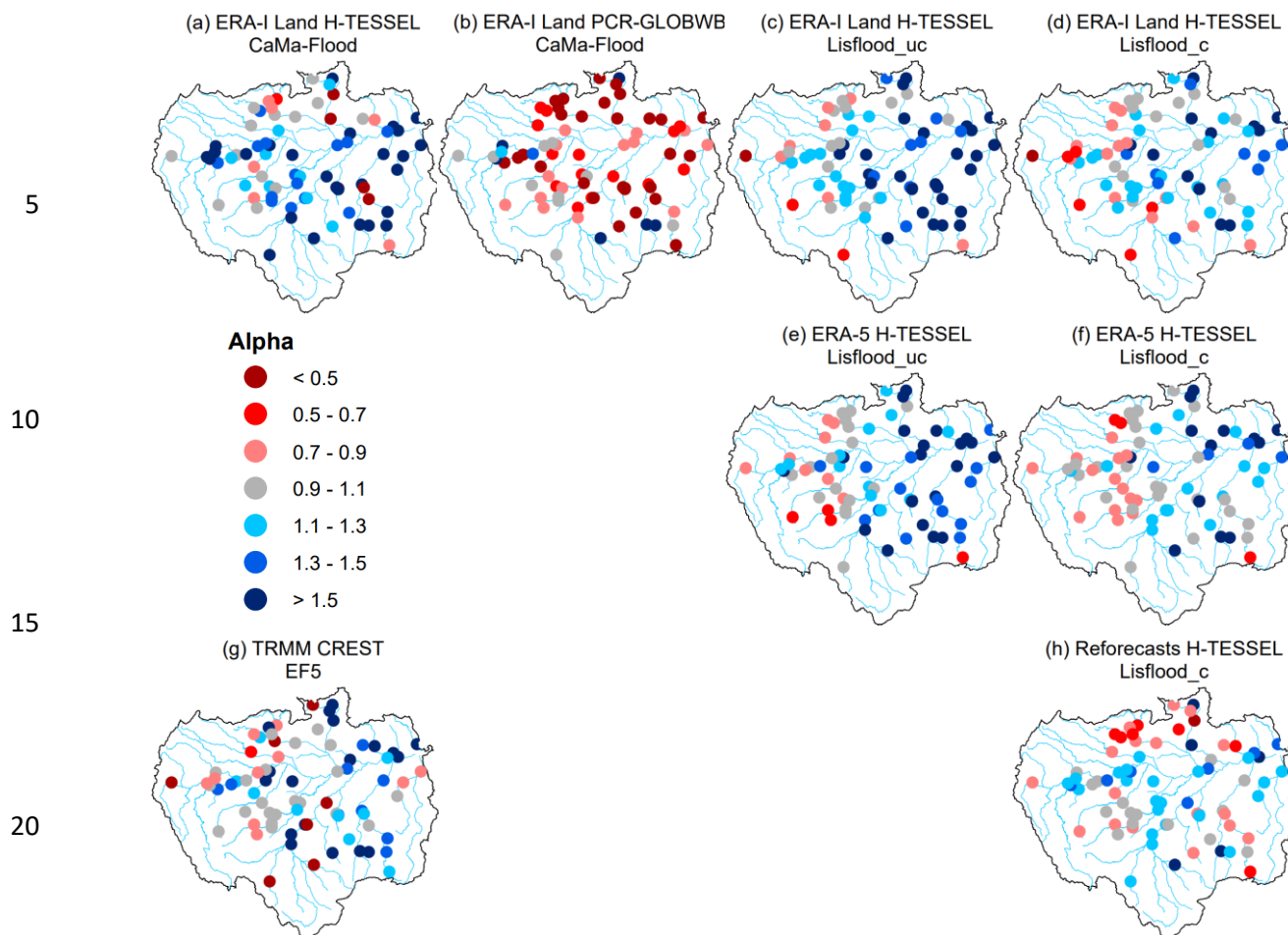
Figure 4: Alpha (i.e. variability) component of the KGE at 75 hydrological gauging stations for all simulations for the period 1997-2015 and 2004-2015 for CREST EF5 (g). Blue circles indicate that the variability in the simulated time series is higher than that of the observed while red circles show the opposite effect. Values closer to one indicate better model performance (i.e. grey circles).
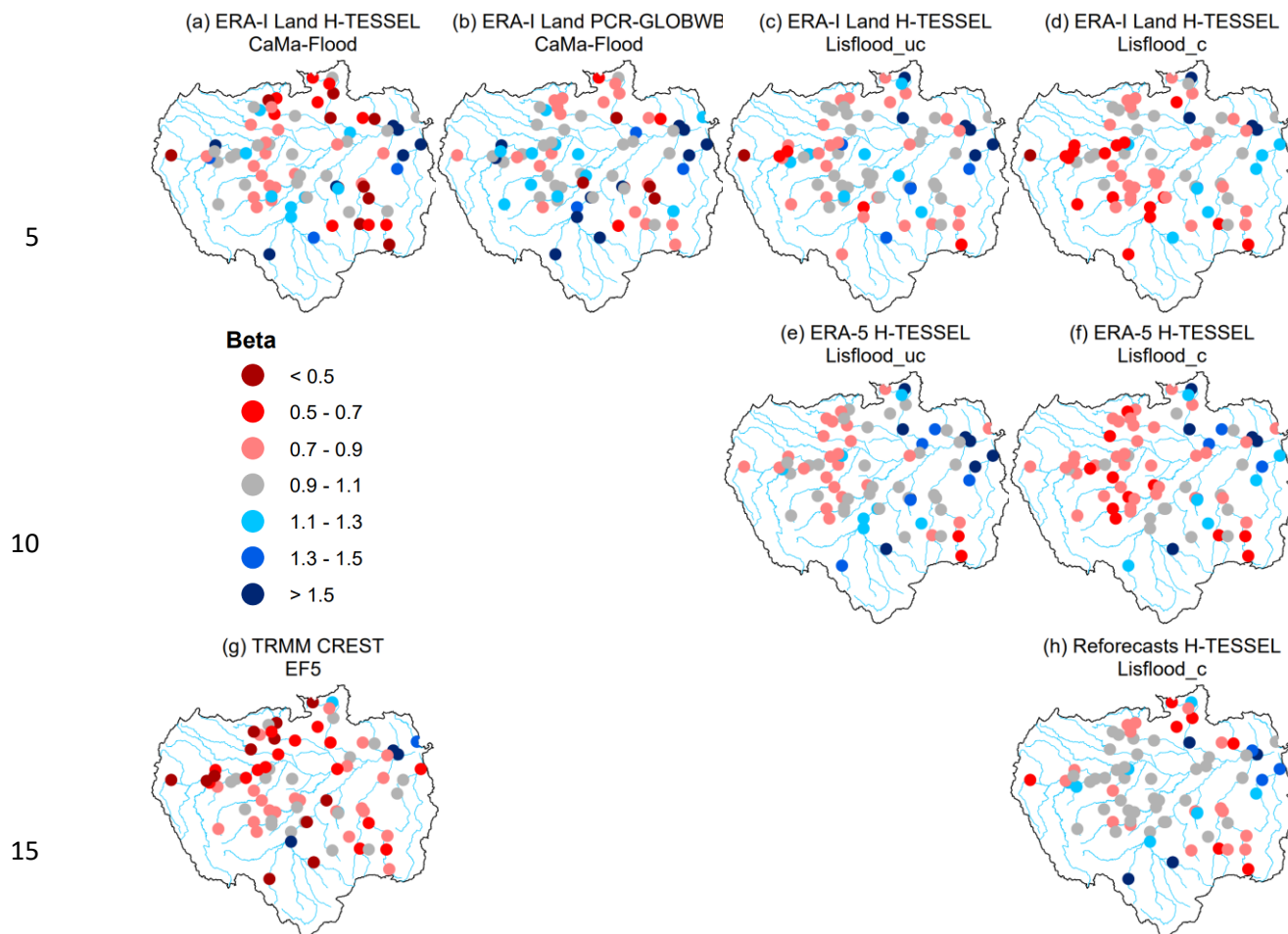
Figure 5: Beta (i.e. bias ratio) component of the KGE at 75 hydrological gauging stations for all simulations for the period 1997-2015 and 2004 -2015 for CREST EF5 (g). Blue circles indicate that the bias in the simulated time series is higher than that of the observed while red circles show the opposite effect. Values closer to one indicate better model performance (i.e. grey circles).
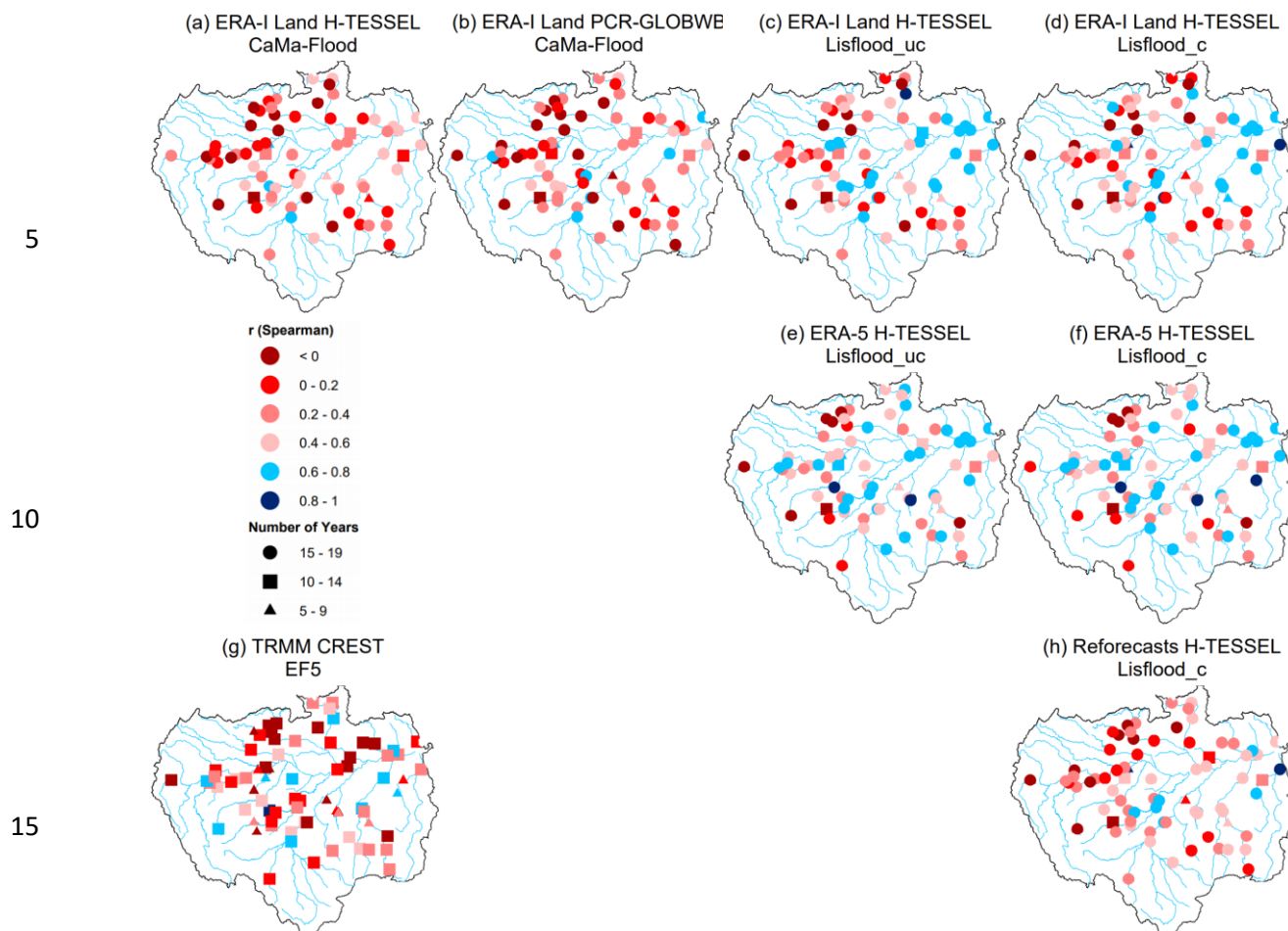
Figure 6: Spearman's ranked correlation coefficients for observed against simulated annual maximum discharge at 75 hydrological gauging stations for all simulations for the period 1997-2015 and 2004-2015 for CREST EF5 (g). Values exceeding 0.6 considered skilful (i.e. blue shapes). Number of overlapping years of data between observations and simulations are denoted by different shapes (e.g. a circle for 15-19 years of overlapping data).
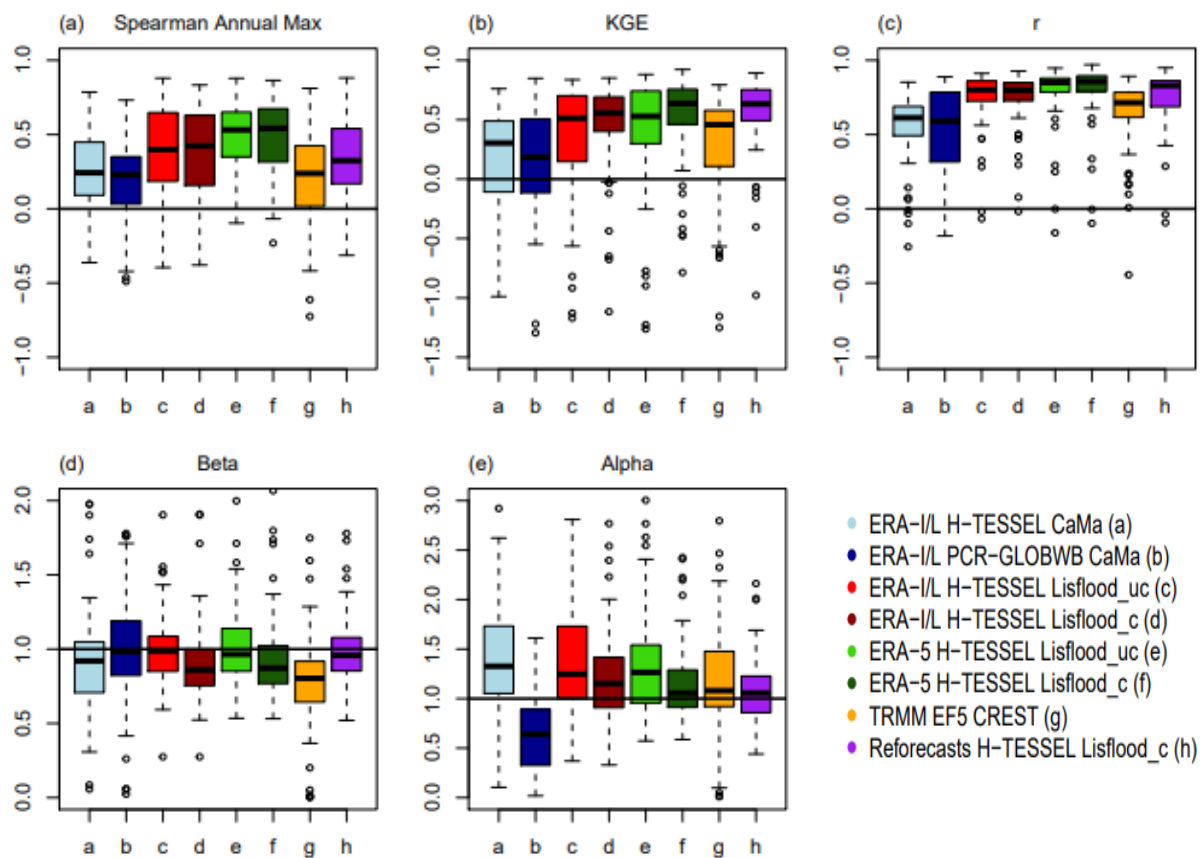
Figure 7: Boxplots showing the distribution of scores for the (a) Spearman correlation coefficient (annual maximum), (b) KGE, (c) KGE Pearson's rho, (d) KGE beta and (e) KGE alpha for all simulations.

Table 2: Mean scores for the 75 hydrological gauging stations for all metrics.

Model Runs	Spearman Annual Max Correlations	KGE	r (Pearson's)	Beta	Alpha
ERA-Interim Land H-TESSEL CaMa-Flood	0.25	0.03	0.57	0.98	1.53
ERA-Interim Land PCR-GLOBWB CaMa-Flood	0.19	0.10	0.53	1.12	0.74
ERA-Interim Land H-TESSEL Lisflood_uc	0.37	0.23	0.75	1.04	1.51
ERA-Interim Land H-TESSEL Lisflood_c	0.37	0.37	0.75	0.92	1.31
ERA-5 H-TESSEL Lisflood_uc	0.48	0.27	0.79	1.09	1.47
ERA-5 H-TESSEL Lisflood_c	0.48	0.41	0.80	0.97	1.28
TRMM CREST EF5	0.21	0.16	0.65	0.78	1.32
Reforecasts H-TESSEL Lisflood_c	0.33	0.53	0.76	1.00	1.10
Mean across models	0.34	0.26	0.70	0.99	1.28
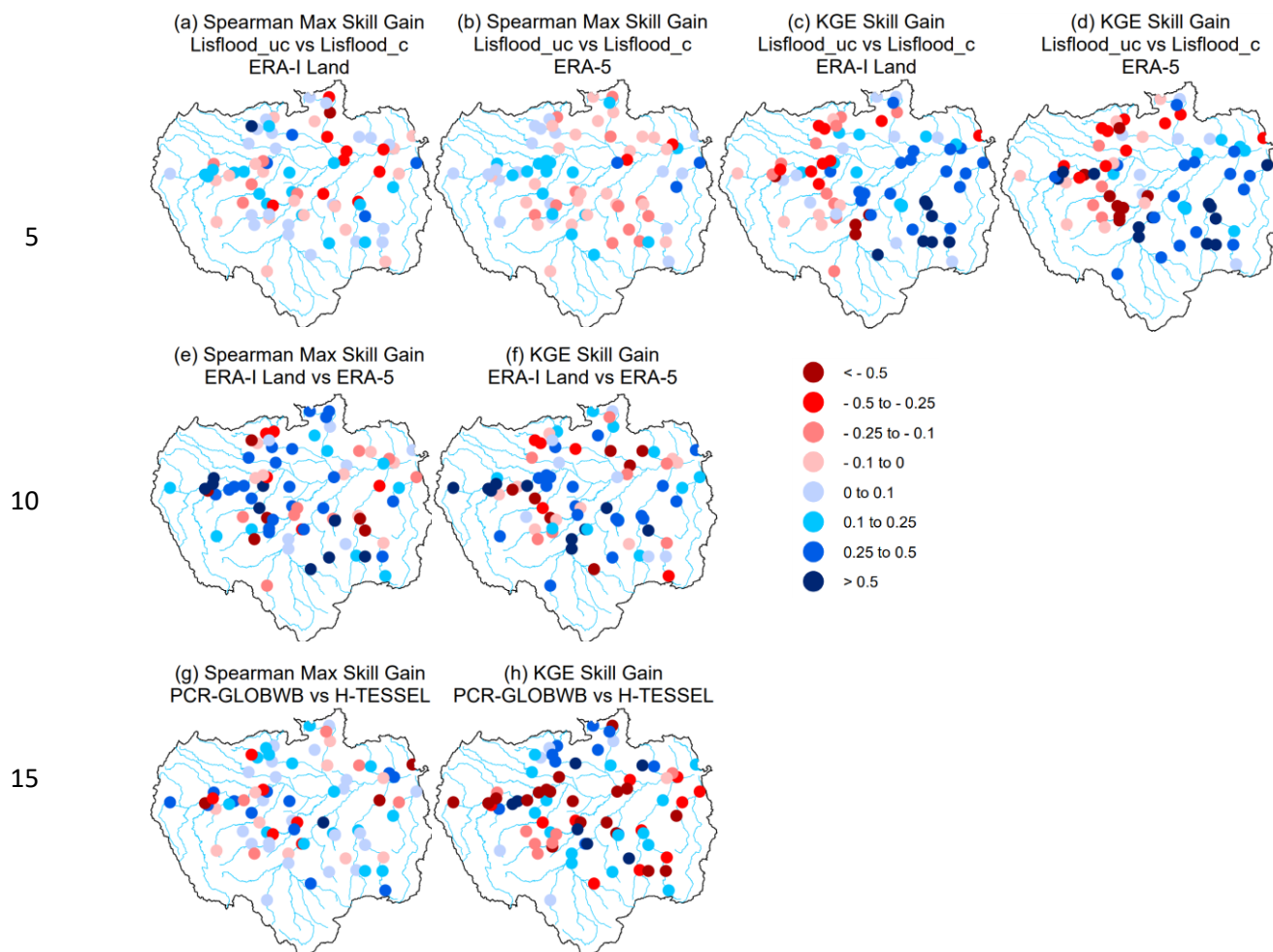
Figure 8: Relative improvement in skill at each gauging station for Spearman annual maximum correlations and KGE values (i.e. skill scores). (a-d) show relative gain or loss in skill when using the newly calibrated Lisflood run (Lisflood_c) relative to the uncalibrated model run (Lisflood_uc) using precipitation forcing from both the ERA-Interim Land and ERA-5 reanalysis products. (e-f) show relative gain or loss in skill when using ERA-5 as opposed to ERA-Interim Land. (g-h) show relative gain or loss in skill when using the LSM H-TESSEL rather than the hydrological model PCR-GLOBWB. All scores are calculated using the skill scores in Eq. (1). Red indicates a decrease in skill whereas blue represents an increase.
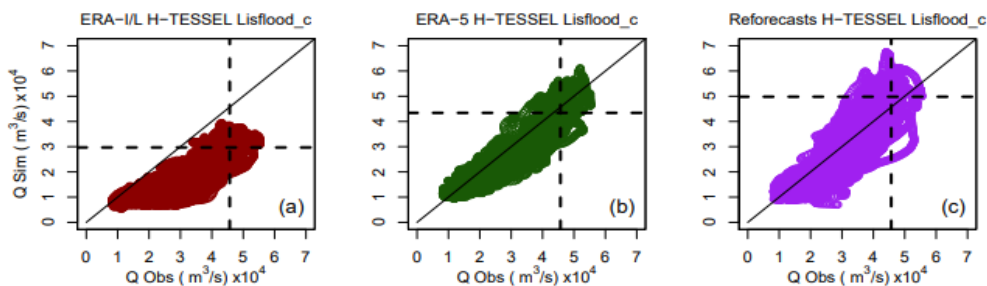
Figure 9: Scatterplots of observed against simulated river flow at the Tamshiyacu gauging site, Peru (*4*). For (a) ERA-Interim Land, (b) ERA-5 and (c) ECMWF 20-year reforecasts forced through the calibrated Lisflood routing model. Dashed black lines indicate the observed and simulated 90th percentile of river flow. For the period 1997-2015.